RF Tunable Resonators and Filters

by

Marco Iskander

A thesis
presented to the University of Waterloo
in fulfillment of the
thesis requirement for the degree of
Master of Applied Science
in
Electrical and Computer Engineering

Waterloo, Ontario, Canada, 2014

AUTHOR'S DECLARATION

I hereby declare that I am the sole author of this thesis. This is a true copy of the thesis, including any required final revisions, as accepted by my examiners.
I understand that my thesis may be made electronically available to the public.

Marco Iskander

Abstract

The recent remarkable growth in the telecommunications industry has caused a huge advance in filter technology. The new communication systems demand stringent filters with high specifications, low costs, compact features, and the ability to accommodate multiple wireless standards (2G, 2.5G, 3G, WiMAX, Mobile WiMAX, LTE and LTE-A). In order to realize a multi-standard RF front end and cover all frequency bands, a transceiver requires a customized RF device that includes tunable filters.

The main building block of any tunable filter is a tunable single resonator. The thesis introduces two novel techniques to extract an equivalent circuit model for RF resonators. Both techniques are successfully tested and validated for different case studies. Using a systematic approach, the lumped element technique can be used to relate the EM model to an adjusted parallel RLC model that takes into consideration the input coupling. The node-to-node technique is based on using a transmission line equivalent to model combline resonators. Several examples are used to apply the technique to gain more insight into understanding and thus improving resonator performance.

The thesis also presents the design and implementation of a high-Q bandpass filter using the proposed angular tuning technique that maintains a constant Q value over a relatively wide tuning range. The traditional technique for tuning combline filters is achieved by changing the gap between the post and the tuning disk. Such a technique is known to yield a Q value that degrades considerably at the lower edge of the tuning range. The proposed angular tuning technique shows a 25% improvement in the Q value at the lower edge of the tuning range, in comparison to what is typically achieved using the traditional tuning technique. Using the proposed angular tuning technique, a 1% bandwidth 2-pole filter is designed, fabricated, and tested with a 430MHz tuning range at a center frequency of 3.6 GHz. The filter is integrated with miniature piezoelectric motors, demonstrating an almost constant insertion loss over the tuning range.

Acknowledgements

First and foremost, I would like to thank God for guiding me throughout these two years and through my entire life. As well, I would like to express my sincere thanks and appreciation to my supervisor, Professor R. R. Mansour, for his mentorship, guidance, encouragement and full support. I would also like to thank Prof. Safieddin Safavi-Naeini and Prof. Omar Ramahi for reviewing my thesis.

In addition, I wish to thank the members of the Centre for Integrated RF Engineering at the University of Waterloo, who were my friends and colleagues for the last two years. Special thanks go to Mostafa Azizi for his valuable technical guidance, Sormeh Setoodeh for sharing her expertise in RF measurements, and Bill Jolley for offering his experience and expertise with RF measurement and assembly. I would also like to thank Mitra Nasresfahani for her great cooperation in doing the RF measurements. Thanks go as well to my officemates, Geoffrey Lee, Dezireh Shojaei and Alborz Rezazadeh.

And most importantly, my deepest appreciation goes to my family, whom I love and cherish dearly. I would like to thank my father, who invested in our education; my departed mother, who is definitely praying for us; my step-mother, who looked after us since our childhood; and my brothers, for always being there for me. I would also like to thank my fiancée for her support, patience and unconditional love.

Last but not least, I would like to thank my dear friends who have enriched my life in so many pleasant and unexpected ways.

Dedication

To my beloved departed mother and grandmother

To my beloved family

And to my dear fiancée

Table of Contents

List of Figures

List of Tables

Chapter 1

Introduction

1.1 Motivation

The recent remarkable growth in the telecommunication industry has sparked a surge in novel filter technology [1]. These new communication systems demand stringent filters that feature high specifications, low cost and compact sizing. The filters should also accommodate multiple wireless standards (2G, 2.5G, 3G, WiMAX, Mobile WiMAX, LTE and LTE-A). In order to realize a multi-standard RF front end and cover all the different frequency bands, the transceiver requires a customized RF device that includes tunable filters.

One unique challenge in designing tunable filters is to maintain the best achievable performance over the tuning range. Extensive research investigations have been done to devise a reconfigurable/tunable RF filter structural design that has high energy efficiency, high tuning speed, excellent linearity, and low loss/or high-Q over the tuning range [2]. Many performance parameters, such as bandwidth (BW), return loss (RL) and Q value or insertion loss (IL), change as the filter is tuned from one center frequency to another. For most of the applications, maintaining good filter performance over the tuning range is much more important than getting a perfect filter at a certain band but giving an unacceptable performance at the edge of the tuning range.

Various tuning techniques have been developed to construct tunable filters, the most common of which are mechanical tuning and electronic tuning. In terms of quality factor, power-handling capability and linearity, mechanical tuning outperforms the other tuning techniques. However, mechanically tunable filters have limited applications due to their bulky size, heavy weight, and low tuning speed.

Current mechanically based tuning techniques rely on inserting a tuning element (screw or disk) and varying its penetration inside the cavity by having the tuning element shift upwards and downwards. In this traditional approach, the Q value starts high and degrades as the filter is tuned to the lower edge of the tuning range. Moreover, moving the tuning element up and down requires the use of a motor with a special mechanism to allow for vertical movement and to leave room for the tuning element stroke. This adds considerable overhead to both the overall filter mass and the volume.

Due to these drawbacks, time and effort need to be invested in designing, understanding and optimizing a single tunable in order to achieve high performance tunable filters. The equivalent circuit model for resonators can be extracted to help researchers understand much of the information about the resonator and its tunability and also give them an idea about the possible ways to improve it. The resonator model should be developed to account for tunability and be directly and clearly related to the actual model from a physical perspective.

1.2 Objectives

The main objectives of the proposed research are:

- Developing an equivalent circuit model for 3D coaxial resonators.

- Developing an efficient mechanically based tuning technique to limit degradation in the Q value, allowing for a constant insertion loss over the tuning range for bandpass combline filters.

- Minimizing the overhead in the volume and mass associated with mechanically tuned filters that require motors to perform automatic tuning.

1.3 Thesis Outline

Following the motivation and objectives given in Chapter 1, Chapter 2 presents an overview of the various filter tuning techniques available in the literature and the advantages and disadvantages of each technique. The third chapter demonstrates approaches to extract an equivalent circuit model for a single microwave resonator. Chapter 4 presents the design, simulation, and experimental results for a tunable filter using the proposed technique. Finally, a brief summary of the contributions of the thesis, along with an outline of proposed future research, are given in Chapter 5.

Chapter 2

Literature Survey

In this chapter, an overview of tunable microwave band-pass filters is presented and recent progress in the performance of various tunable filters is reported. In section 2.1, various tuning techniques are presented. Section 2.2 discusses different ways suggested in the literature to develop an equivalent circuit model of a single microwave resonator.

2.1 Tunable Filters

All tunable filters presented in this section fall into three main categories: mechanically tunable, magnetically tunable, and electronically tunable [3].

2.1.1 Mechanically Tunable Filters

In terms of the Q-factor, power-handling capability and linearity, mechanical tuning is superior to magnetic and electronic tuning. However, low tuning speed, bulky size and heavy weight are major disadvantages of mechanical tuning [4].

Waveguide and coaxial resonators are the resonators typically used for mechanical tunable filters [3]. The tuning of these types of mechanically tunable bandpass filters is accomplished manually or by electronic motors.

Fouladi et al. presented 6-pole filters tuned from 2.535 GHz to 2.635 GHz using piezomotors [4]. The maximum insertion loss is less than 2.3dB over the tuning range and the return loss is better than 16dB. However, even though the rejection level of 25dB at 5-MHz offset by the passband is achieved for the designed filter, the motors add sizeable overhead weight and volume on top of the filter. Figure 2.1(a) shows the motor setup of [4].

Loading the tunable bandpass filter by dielectric material helps reduce the filter size without sacrificing too much of the Q, as was developed in [5] [6] [7]. Figure 2.2(a) illustrates a 4-pole dielectric resonator loaded tunable bandpass filter. The dielectric tunable bandpass filter presented by Chen et al. [5] displays good tuning properties in terms of filter size, tuning range, and loss. However, the filter's tuning speed is very low due to the tuning screw-like configuration. In [6], two dielectric resonators were employed to construct a bandpass filter, with two other dielectric resonators serving as tuning disks. By moving the tuning disk close to the resonators, the resonant frequency is reduced due to the extra loading effect of the dielectric tuning disks. The center frequency can be tuned continuously from 4.6 to 4.8 GHz without significant changes in its return loss or bandwidth, as shown in Figure 2.2(b). The insertion loss varies between 0.85 and 1.15dB, corresponding to the unloaded Q of 5200 and 4700, respectively, over a 200-MHz tuning range.
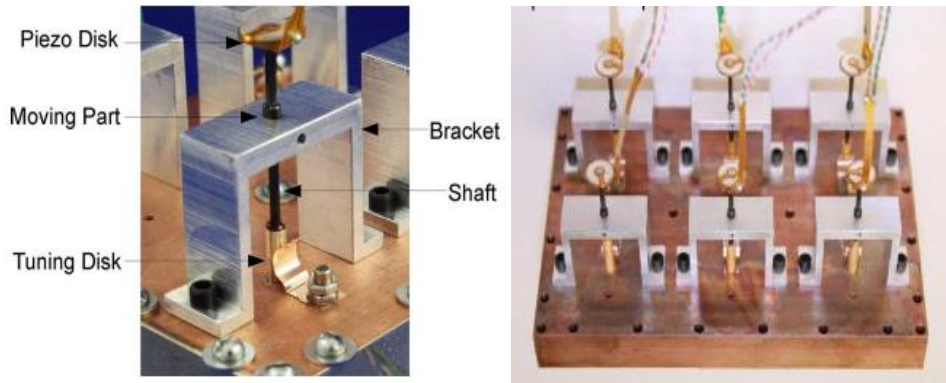
(a)
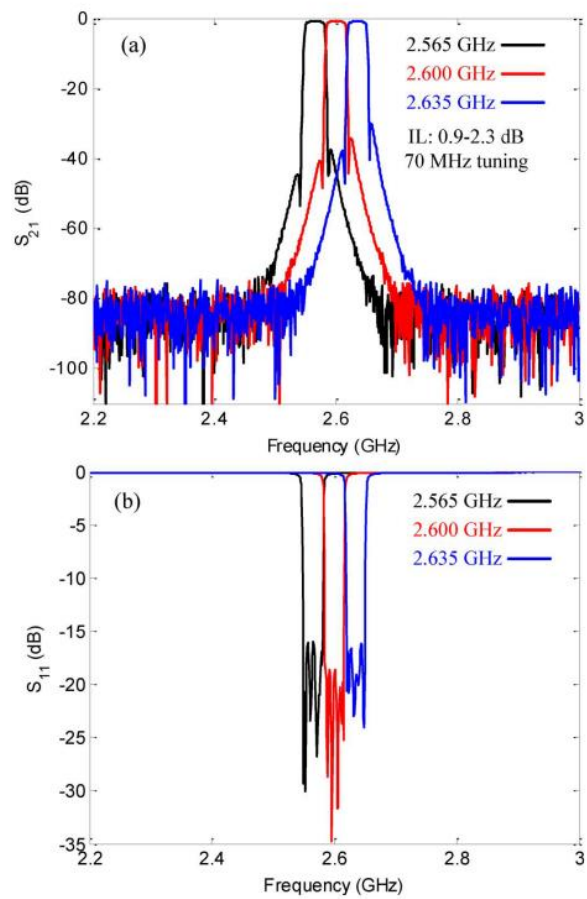
(b)

Figure 2.1 (a) Motor setup; (b) measured S-parameters, as in [4]
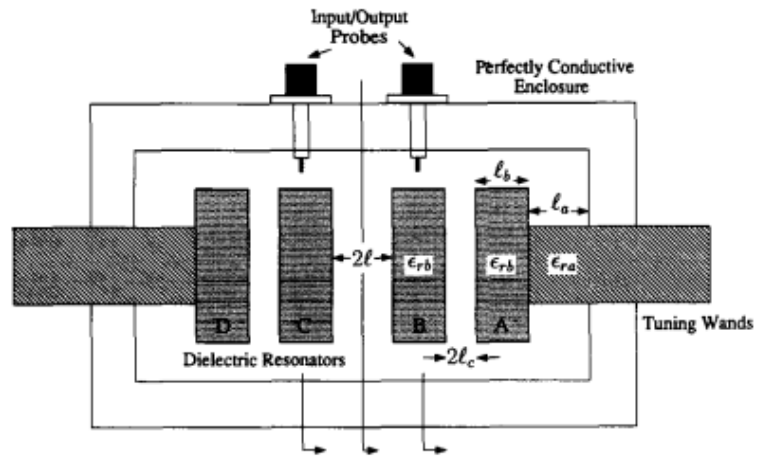
(a)
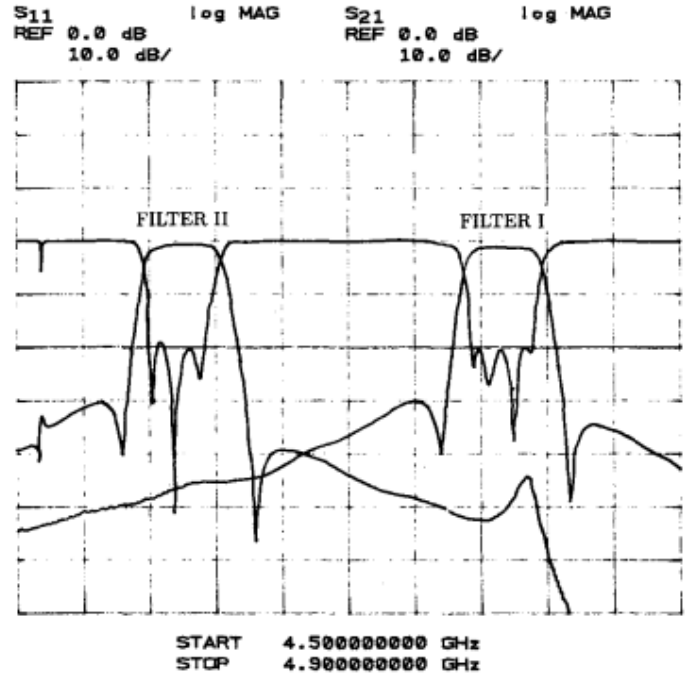
(b)

Figure 2.2 (a) Filter configuration; (b) measured S-parameters, as in [5]

Mechanical tuning techniques have been implemented not only in cavity tunable filters, but also in planar tunable filters such as microstrip line filters [8], LTCC filters [9], and HTS filters [10]. One example of a mechanically tuned planar bandpass filter [8] is shown in Figure 2.3(a). A dielectric perturber attached to a piezoelectric actuator is suspended above a microstrip bandpass filter. When voltage is applied to the piezoelectric actuator, it can move the perturber up or down along the Z axis. When the dielectric perturber is moved closer to the filter, the dielectric constant of the substrate is effectively increased, which in turn lowers the center frequency of the filter. Figure 2.3 (b) shows the measured S-parameters of the filter.
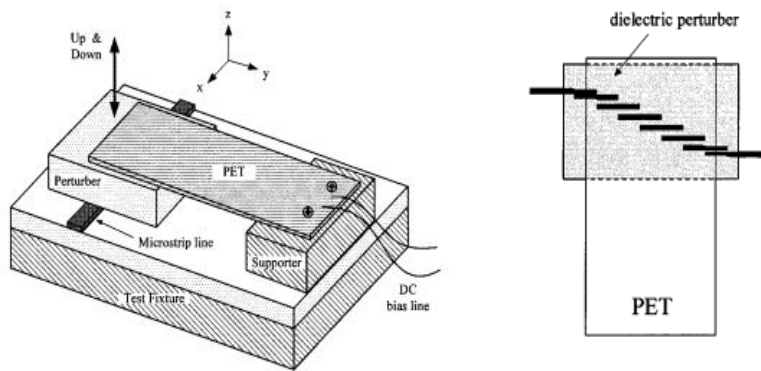
(a)
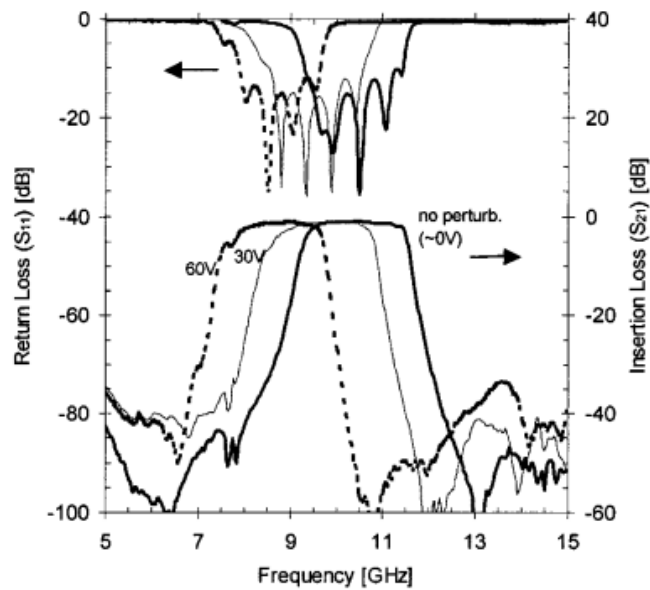
(b)

Figure 2.3 (a) Filter configuration; (b) measured S-parameters, as in [8]

2.1.2 Magnetically Tunable Filters

The most widely held examples of magnetically tunable filters are filters with Yttrium-Iron-Garnet (YIG)-based resonators. The ferromagnetic resonators of these filters enable them to be tuned by applying an external DC magnetic field and variation of the ferromagnetic resonant frequency of YIG spheres. Although YIG filters have low insertion loss and high quality factor (Q) resonators, they suffer from large power consumption (0.1-1 W) [11]. Another disadvantage of YIG filters is their non-planar structure, which prevents their wide application in modern communication systems.

Krukpa et al. constructed magnetically tunable filters using axially magnetized ferrite elements, as shown in Figure 2.4. The filter operates at 2 GHz, with a tuning range of at least 10 MHz and a *Q* in the order of 10,000 [12]. The insertion loss is less than 0.4dB, as shown in Figure 2.4. Despite these impressive results, the filter suffers from large power consumption (4W).
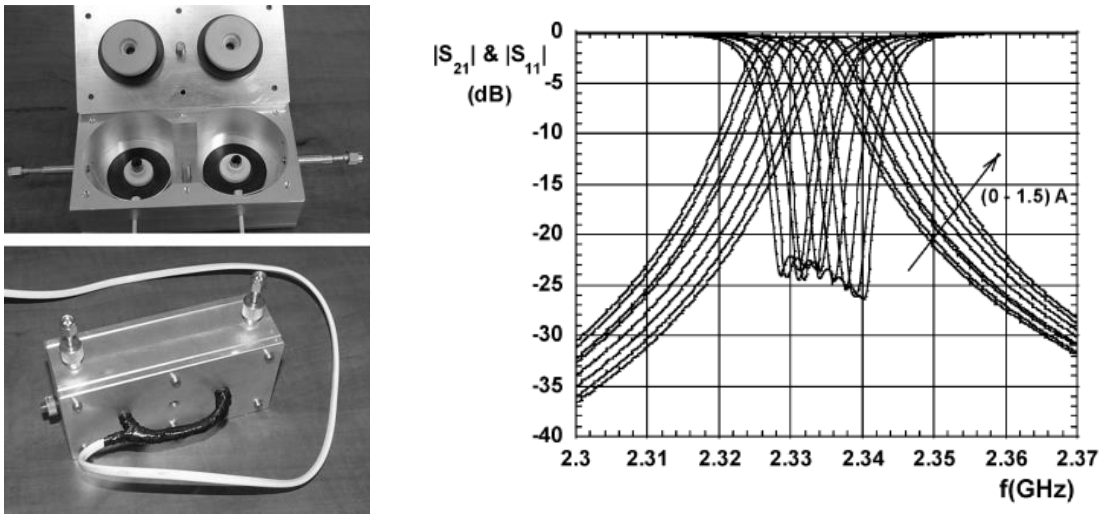
Figure 2.4 Filter configuration and measured S-parameters, as in [12]

2.1.3 Electronically Tunable Filters

Electronically tunable filters come in three different types: varactor diodes, Barium Strontium Titanate (BST), and Radio-Frequency Micro-Electro-Mechanical Systems (RF MEMS).

2.1.3.1 Varactor Diode

The varactor diode-based concept is based on changing the depletion region width, which results in changing the capacitance. A reverse-bias DC voltage is utilized to perform this change. Despite the fact that these filters have zero power consumption and relatively fast tuning speed, they suffer from a moderate *Q* of the resonators [13].

Brown et al. presented an electronically tunable filter by applying suspended substrate design and varactors as the tuning element [14]. The filter has a 60% center frequency tuning bandwidth from

700MHz to 1.33 GHz and the insertion loss is less than 3dB for half of the tuning range. However, the filter suffers from severe bandwidth uncontrollability (fractional bandwidth varies from 14% to 0.5% as the center frequency is tuned from 1 GHz to 700MHz). The considerable effect of the diode series resistance on Q was also investigated in the paper.

Sanchez-Renedo et al. demonstrated a tunable combline filter with additional transmission zeros by applying multiple couplings between the source/load and resonators [15]. The center frequency tuning range is from 400 MHz to 800MHz. The filter suffers from high insertion loss, especially at lower center frequencies as well as bandwidth uncontrollability.

Huang et al. presented a varactor tuned dielectric resonator filter [16]. The varactor is mounted on a PCB circuit board that is connected outside the filter housing. The center frequency is tuned from 4.98 to 5.28GHz, with the insertion loss changing from 3.4 to 1.47dB. The return loss shows some degradation, especially in high center frequencies. Figure 2.5 shows the 3D view of the single varactor-tuned dielectric resonator and measured S-parameters for its corresponding 2-pole filter.
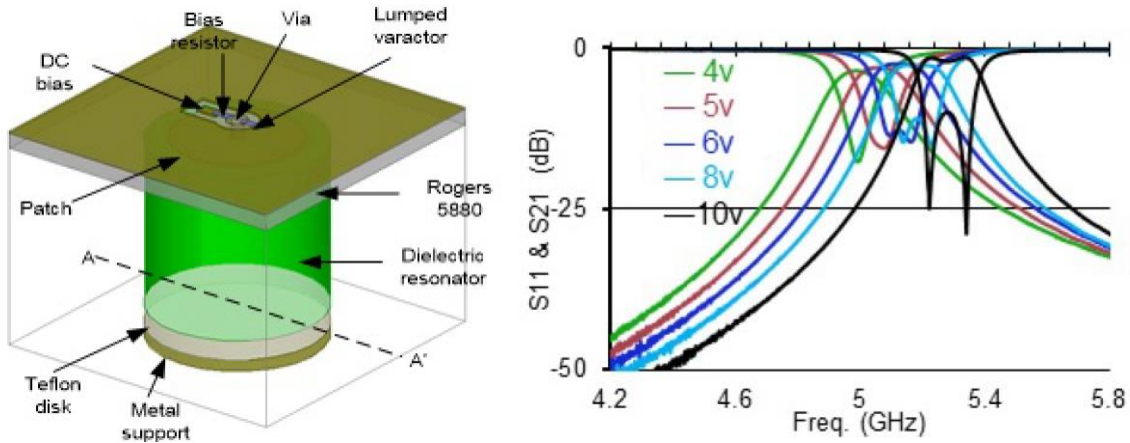
Figure 2.5 A 3D view of a varactor-tunable dielectric resonator and the measured S-parameters for its corresponding 2-pole filer, as in [16]

2.1.3.2 BST

A ferroelectric thin-film BST tunable capacitor is the fundamental element of BST tunable filters. An electric field can change the relative dielectric constant of ferroelectric materials. The major advantages of BST filters are that they are planar, easy to integrate, and have zero power consumption [17]. However, they also suffer from poor linearity and moderate Q.

In [18], Sanderson et al. presented a tunable IF filter by employing thin-film BST varactors. The filter center frequency is tunable from 30 to 88 MHz in three separate switch-selectable bands. The fractional bandwidth is relatively constant in the tuning range, and the insertion loss is less than 5dB for the entire tuning range.

8

Chun et al. demonstrated a bandpass tunable bandwidth filter by employing an interdigital BST varactor [19]. The center frequency of this filter is 1.8 GHz and the 3-dB bandwidth is tunable from 276 to 318MHz.

Nguyen et al. applied high-Q, tunable ICs to demonstrate a tunable bandpass filter [20]. Two filters were presented: a 2-pole tunable filter with a tuning range from 300 to 470MHz and an insertion loss less than 2dB over the entire tuning range; and a 3-pole filter with center frequency tuning from 230 MHz to 400 MHz and an insertion filter of less than 2.5dB for the entire frequency range.

In [21], Nath et al. presented a tunable third-order microstrip combline bandpass filter that used BST varactors and was fabricated on a sapphire substrate. Changing the bias from 0 to 200Volts varied the center frequency of the filter from 2.44 to 2.88 GHz and achieved a 1-dB bandwidth of 400MHz. The insertion loss varied from 5.1dB at zero bias to 3.3dB at full bias, while the return loss was better than 13dB over the range.

2.1.3.3 RF MEMS

The tuning element of an RF MEMS tunable filter is usually a capacitance network based on RF MEMS. Applied DC voltage is required to achieve variations in the capacitance by employing micrometer level movements. Low insertion loss, high linearity, and low power consumption are some advantages of these filters. On the other hand, as they need a high voltage drive to operate (25-90 V), relatively more complex circuitry for high-voltage drive circuits is required.

Entesari et al. presented a 4-bit, 2-pole tunable filter by employing switched capacitors, metal contact switches, and fixed-value capacitors [22]. The Radant-MEMS switches are used on top of FR-4 filter substrate; the measured insertion loss is 3–5dB at 25–75 MHz; the relative bandwidth is $4 \pm 1\%$, the return loss is better than 13dB, and the measured IIP3 of the tunable filter is greater than +65dBm. A resonator Q of 52–75 was measured over all tuning states.

Reines et al. developed a high-Q filter by employing suspended strip-line configurations. They developed the first suspended three-pole high-Q tunable combline RF MEMS tunable filter with frequency coverage of 1.6–2.4 GHz, built on a quartz substrate [23]. The essential element for a 3-pole low-loss filter is a high-Q resonator and the suspended topology is chosen to fulfill the Q requirement. Both the resonators and the input/output matching networks are tunable. The insertion loss of the filter is 1.34–3.03dB over the tuning range and a 3-dB bandwidth of 201–279 MHz. The quality factor is tunable and its value is 50–150 over the frequency range.

In [24], Park et al. employed a high-Q 3-bits orthogonally-biased RF MEMS capacitance network and built a low-loss 3-bit tunable filter. The orthogonal biasing networks ensure high-Q operation because of a very low RF leakage through the bias lines. The measured filter has an insertion loss of 1.5–2.8dB with a 1-dB bandwidth of $4.35 \pm 0.35\%$ over the 4–6 GHz tuning range. The tunable Q is 85–170 and can be improved to 125–210 with the use of a thicker bottom electrode for the RF MEMS capacitive switch. At 5.91 GHz, the measured IIP3 is greater than 40dBm while 1-dB power compression point is greater than +27.5dBm.

An attempt to achieve constant absolute bandwidth was done in [25], where El-Tanani et al. developed a tunable filter fabricated on ceramic substrates (with a dielectric constant of 9.9) for

miniaturization. The design is based on corrugated coupled-lines. Because the 3-bit tuning network is fabricated using a digital/analog RF MEMS device, it can provide a large capacitance ratio and continuous frequency coverage. The insertion loss of 1.9-2.2dB at 1.5-2.5GHz is measured in narrowband (bandwidth of 72 ± 3 MHz) and wideband (bandwidth of 115 ± 10MHz) 2-pole filters. The power handling is 25dBm and the IIP3 is greater than 35dBm. A Q-factor of 85–165 was reported for this filter.

2.2 Resonator equivalent circuits

Very little research has been carried out thus far into extracting an equivalent circuit model for a single microwave resonator. Of that which has been done, most use lumped RLC models to describe the resonance frequency and the *Q*. The drawback of this model is that it does not relate clearly and directly to the actual model of the resonator. It also describes only the mode of interests without including any other modes and is valid only for a small bandwidth around ω_o. In some cases, the circuit model of the resonator is needed so that we can connect it to an external loading circuit and check the performance. This is not possible if the model does not relate directly to the physical resonator, as in most lumped-element-based models.

Owens [26] proposed an approach to derive the equivalent circuit by getting an entirely consistent set of circuit parameters. The study used parallel resonance and related its parameters (R, L and C) to the stored energy (W), average power loss (WL), maximum stored charge (q) and angular resonance frequency (ω). To use this method W, WL, Q and ω should be known for the cavity, which is not always the case (especially for non-traditional configurations). Also, for higher-order modes, equating the charge is complex [26]. In addition, it is worth noting that this way doesn't take other resonance modes into consideration. Finally, the input coupling associated with probe is not modeled. The paper presented the case of a cylindrical (E010) and rectangular waveguide (H10) resonator as an example.

In the same direction, Toman [27] proposed determining the parallel equivalence of a cylindrical cavity resonator in the TM010 mode. The approach showed agreement in the Q-factor as well as center frequency for using circuit methods and energy consideration. More details can be found in [27].

In [28], Wheless et al. developed an equivalent lumped-element model for a dielectric resonator. An iterative procedure is developed for least square estimation from measured data. The procedure is applicable to large data sets obtained by an automatic network analyzer and uses iterations to obtain fiver parameters. These five parameters are the value of reactance occurring at ωo (X_e), the slope of the linearly growing part of X_e (Q_e), the angular resonance frequency (ω_o), the coupling coefficient (κ), and the unloaded Q-factor (Q_o). The procedure is purely mathematical and is intended to minimize any errors until the measured data fits. Figure 2.6 shows the equivalent lumped circuit model used.

Figure 2.6 Equivalent circuit near ω_o, as in [28]
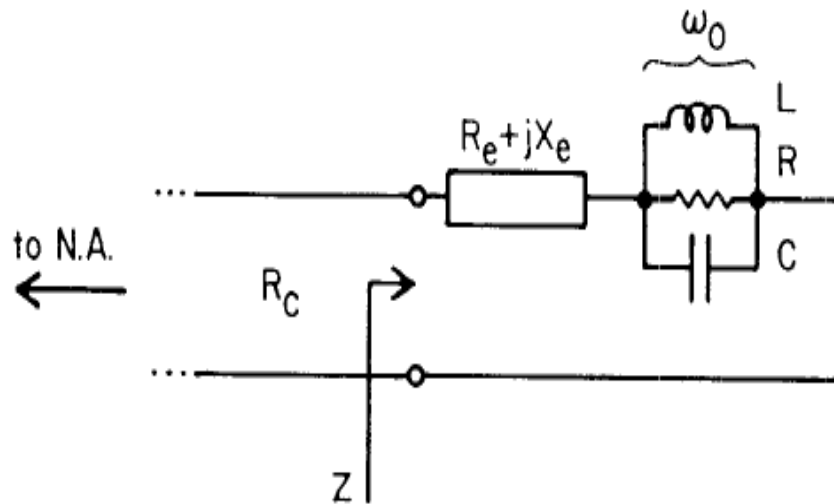
Simion [29] showed an equivalent circuit model for a dielectric resonator that consists of a microstrip line coupled with a dielectric cylinder, as shown in Figure 2.7. The model analytically calculates the components of the circuit and shows a match to experimental results of about 10%.
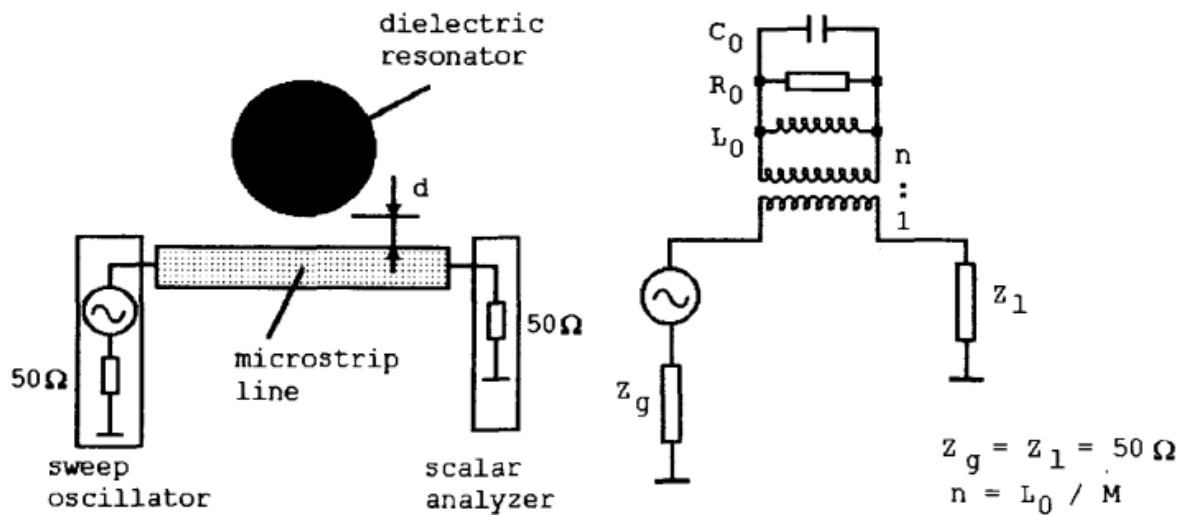
Figure 2.7 Equivalent circuit model for dielectric resonator, as in [29]

Chapter 3

Equivalent Circuit Models for RF Resonators

3.1 Introduction

The basic building block of any filter is a single resonator. When the design of a tunable filter with stringent performance is required, this of necessity implies the need for a high performance single tunable resonator.

Building an EM model of the resonator is considered the first step in designing a tunable resonator. The tunability of the resonator plays a major role in its design, so a tuning element should be used to allow the center frequency tuning. As discussed earlier, tuning can be done mechanically, magnetically or electronically. However, for any of these three methods, a deep understanding of how the tuning works will help in achieving a higher Q performance for the tuning. For instance, if a varactor is connected to a cavity to perform the tuning, the way it is connected and the place it is connected to will greatly affect the Q. Similarly, when a mechanical tuning element is used, the way it moves and the place it is fixed to will have a significant impact on performance.

Developing an EM-based equivalent circuit model can help clarify how a resonator performs. Furthermore, using both EM simulation and a circuit simulator helps a user gain more insight into improving resonator performance. Two methods are proposed in this chapter to obtain an equivalent circuit model of a tunable resonator using: the lumped element technique, and the node-to-node modeling technique:

1- The *lumped element technique* for a tank circuit uses resistance, inductance and capacitance to present the unloaded resonance, preceded by a coupling element (inductance or capacitance). Tuning is modeled by connected tuning elements (a combination of capacitance, inductance and resistance) to the tank circuit to track the change of the center frequency and Q-factor. This technique provides a systematic approach to obtain all of the components' values.

2- The *node-to-node modeling technique* models the resonator as parallel and series transmission lines that are either short-circuited or open-circuited at the ends. The transmission line is coupled at a certain point (depending on the input SMA connector position) to the input by a coupling circuit that depends on the way the SMA connector is inserted (i.e., tapped to the inner conductor or having a gap). Tuning is modeled by adding lumped components that relate physically to changes that the tuning element produces. For example, a change in gap dimensions at the end of a transmission line is modeled as a change in capacitance that is connected at the same location (i.e., end of the transmission line).

It is important to note that, although the circuit model does not precisely match the EM model, the circuit model does help to clarify how the resonator functions and why it performs in that way. This, in turn, assists in optimizing the EM model.

3.2 Lumped Element Technique

A resonator can be viewed as a 1-port network that has a notch in its input reflection coefficient (Γ_{in}) performance. The position of the notch is determined by the resonance frequency, and the sharpness of the notch is described by the loaded *Q*- factor. To obtain the equivalent circuit of a microwave resonator following the definition stated previously, we can use the series or parallel RLC circuit models to get the same resonance frequency and *Q*-factor.

However, although this model fits $|\Gamma_{in}|$, it is not accurate because it does not take into consideration the coupling. For example, the microwave resonator may be under-coupled and the model can be over-coupled, or vice versa. Therefore, to obtain an exact model, the coupling should have the same type and both models should have the same coupling coefficient value (κ) and input impedance Z_{in}[1].

To achieve a model that fits the microwave resonator performance, the loaded resonator is presented with a coupling circuit, followed by an unloaded resonator, as shown in Figure 3.1.
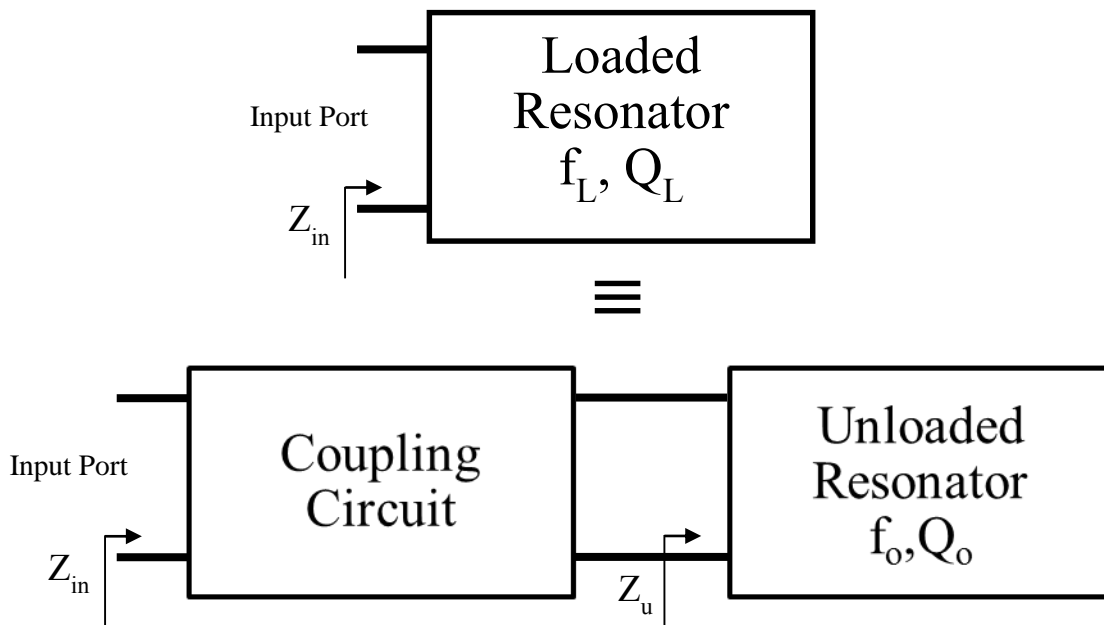
Figure 3.1 Diagram showing the equivalent model of a loaded resonator

In practical terms, a coupling circuit is indispensable for transferring energy between the source and the resonator. The coupling can be presented as resistance in series with either capacitance or inductance. Typically, the resistance is neglected [28].

---

[1] For all of the simulation plots in this chapter, Z_{in} is referred to as Z(1,1), which is the conventional way that ADS and HFSS refer to the input impedance of a 1-port network. Generally, if the port number is 'n', its Z_{in} is referred to as Z(n,n) .

For tank circuit (unloaded resonator), the Z-plane locus (which is the imaginary component of input impedance versus the real component of the input impedance) should have a circular shape that is centered symmetrically around the x-axis. Figure 3.2(a) shows the ADS simulation of an RLC parallel resonance circuit. Figure 3.2(b) shows the Z-plane locus of the circuit, which is presented as a circle, perfectly symmetric around the x-axis.

(a)
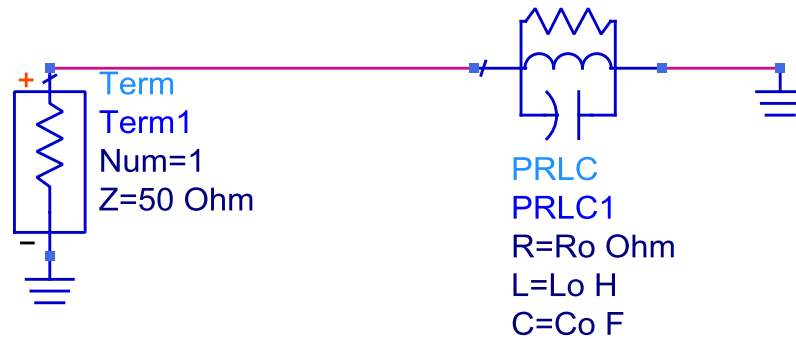
(b)

Figure 3.2 ADS simulation of an RLC parallel resonance tank circuit

Due to the input coupling (coupling circuit), this circle is shifted upward or downward when the coupling is inductive or capacitive, respectively.

3.2.1 Motivation

The challenge consists of two phases:

1. For a microwave resonator, we need to find the equivalent circuit that fits all of its parameters in magnitude and phase. The equivalent circuit consists of four elements:

   a. Coupling element: L_c (if it is inductively coupled) or C_c (if it is capacitively coupled)

   b. Unloaded resonator Resistance: R_o

   c. Unloaded resonator Capacitance: C_o

   d. Unloaded resonator Inductance: L_o

2. Obtaining the equivalent circuit of a tunable resonator can be done by adding more elements (R_{tune} and/or C_{tune} and/or L_{tune}) to track resonator-tuning behavior.

3.2.2 Proposed procedure

1.1.2.2 Finding the coupling element

The procedure starts by finding the coupling element value L_c or C_c. Let us assume that we have a capacitive coupling, as in Figure 3.3.
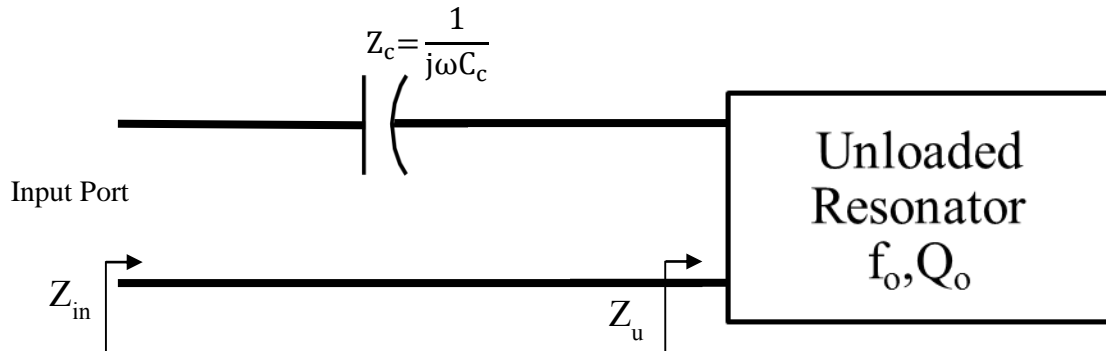
Figure 3.3 Diagram showing the equivalent model of a loaded resonator in capacitive coupling

$$Z_{in} = Z_c + Z_u \tag{3.1}$$

By knowing Z_{in} and also knowing that the unloaded impedance (Z_u) locus should be centered around the x-axis, we can find C_c by trial and error. From Equation 3.1, we can see that subtracting the impedance resulting from C_c from Z_{in} should yield a balanced Z_u locus around the x-axis.

$$\Gamma_u = \frac{Z_u - Z_o}{Z_u + Z_o} \tag{3.2}$$

Furthermore, by knowing Z_o, we can use it to get the unloaded reflection coefficient (Γ_u) from Equation 3.2. From Γ_u, we can get the unloaded center frequency (f_o).

15

3.2.2.1 Obtaining tank circuit parameters (R_o, C_o and L_o)

After compensating for the shift and knowing the coupling element value, by the knowledge of f_o (calculated previously), $Q_o{}^2$ and Z_{in} of the loaded resonator, we can get the parameters (R_o, C_o and L_o):

$$R_o = Max(Real(Z_{in})) \tag{3.3}$$

For parallel resonance,

$$Q_o = \omega_o C_o R_o \tag{3.4}$$

$$\omega_o = \frac{1}{\sqrt{L_o C_o}} \tag{3.5}$$

Equations 3.4 and 3.5 are used to get C_o and L_o, respectively.

3.2.2.2 Allowing for tunability (R_{tune} and/or C_{tune} and/or L_{tune})

More circuit components are added to track changes in center frequency, Q-factor, coupling and Z_{in}. First, the coupling is readjusted in the same way as discussed previously. Then, we modify R_{tune} and/or C_{tune} and/or L_{tune} to get the perfect match of the new circuit.

3.2.3 Case study: Angular tunable resonator

We will begin by presenting the EM model of a novel tunable resonator using the angular tuning technique (to be discussed in detail in Chapter 4) and then explain the proposed procedure for obtaining its circuit model.

3.2.3.1 EM Model

The combline resonator has a cavity of size 40cm × 40cm × 30cm, enclosing a cylindrical post 10mm in diameter and 15mm in height. The tuning element is a 12cm × 18cm rectangular sheet attached to a vertical shaft. As shown in Figure 3.4, the center of the shaft is shifted from the post's center position and the rectangular tuning element rotates radially around the vertical shaft's center. When the angle of rotation changes, the overlap area between the tuning element and the post varies, this in turn tunes the resonator's center frequency and maintains almost the same Q.

---

[2] All Q-factor calculations in this chapter are based on section 11.4 in [33].
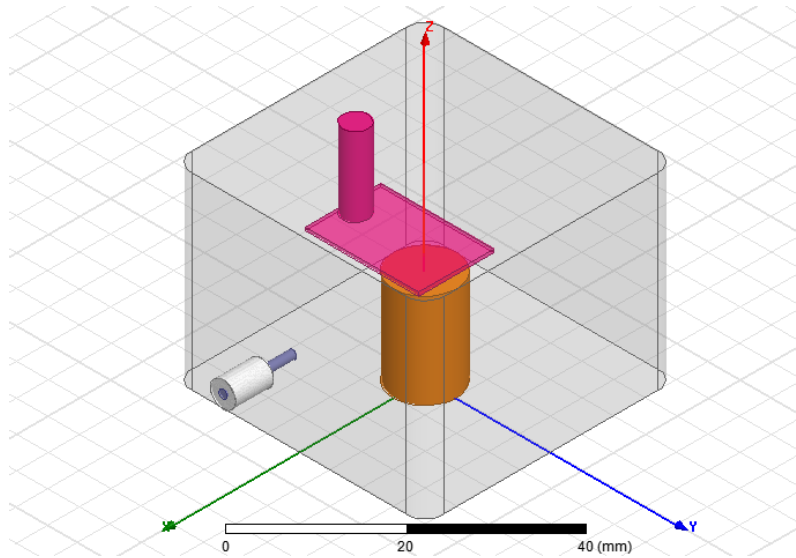
Figure 3.4 EM model of tunable resonator based on angular tuning technique

 S-parameters

Figure 3.5 shows the input reflection coefficient (Γ_{in})[3] of the resonator for different tuning states (angles).

(a)   **(b)**
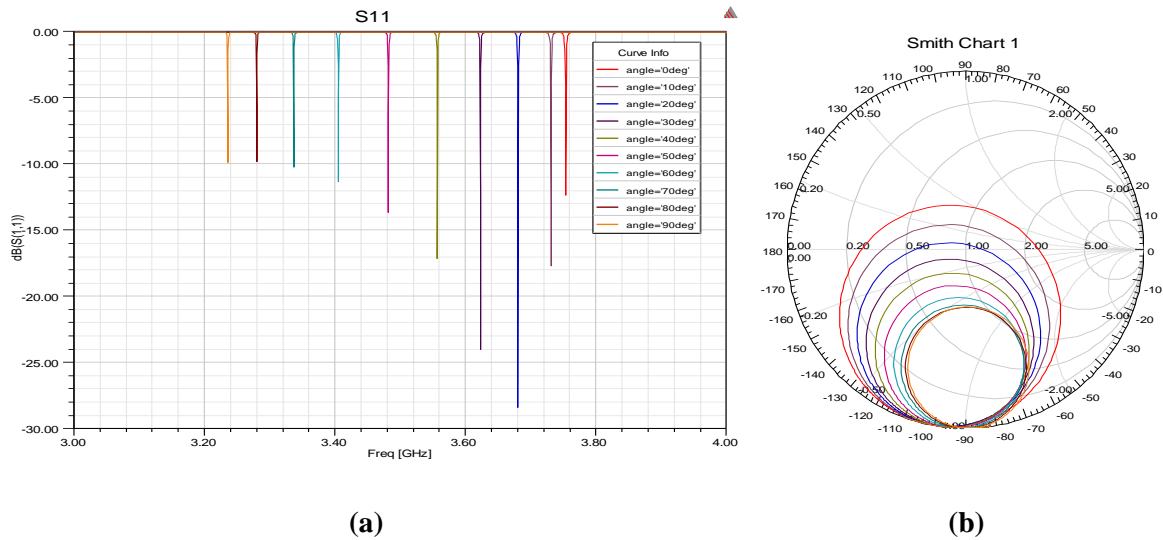
Figure 3.5 Simulated input reflection coefficient for the resonator at different angles:

(a) magnitude in (dB); (b) smith chart

---

[3] For all the simulation plots in this chapter, the input reflection coefficient (Γ_{in}) is referred to as S(1,1), which is the conventional way that ADS and HFSS refer to the input reflection coefficient of a 1-port network. Generally, if the port number is 'n', its Γ_{in} is referred to as S(n,n) .

Z- Parameters and Z-plane locus

Figure 3.6(a) shows the real component of the input impedance Z_{in}. Over the tuning range, the maximum value of the real component of Z_{in} is changing, which means that we will need R_{tune} to account for this change. Figure 3.6(b) shows the imaginary component of Z_{in}. The coupling is not only capacitive but also changes with tuning, so that Cc will also slightly change with tuning.
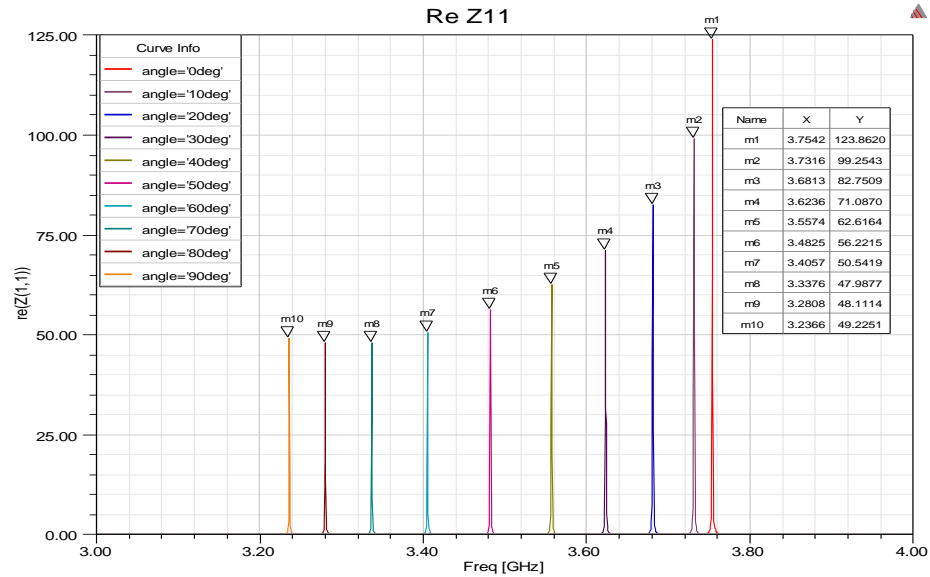
(a)
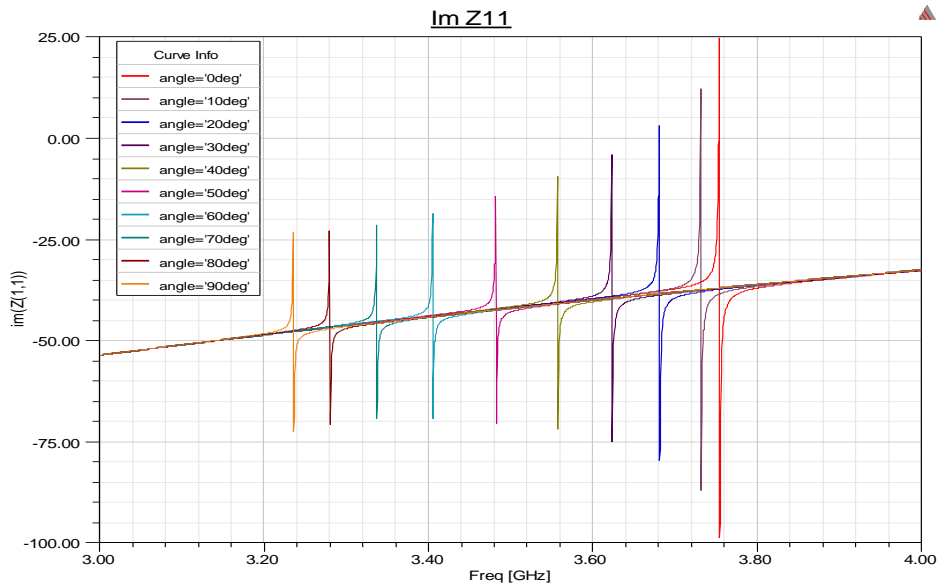
(b)

Figure 3.6 Simulated input impedance for the resonator at different angles:

(a) real component; (b) imaginary component

Figure 3.7 shows the Z-plane locus for different tuning angles. For all the tuning states, the circle is shifted downward, which again means that the coupling is capacitive.
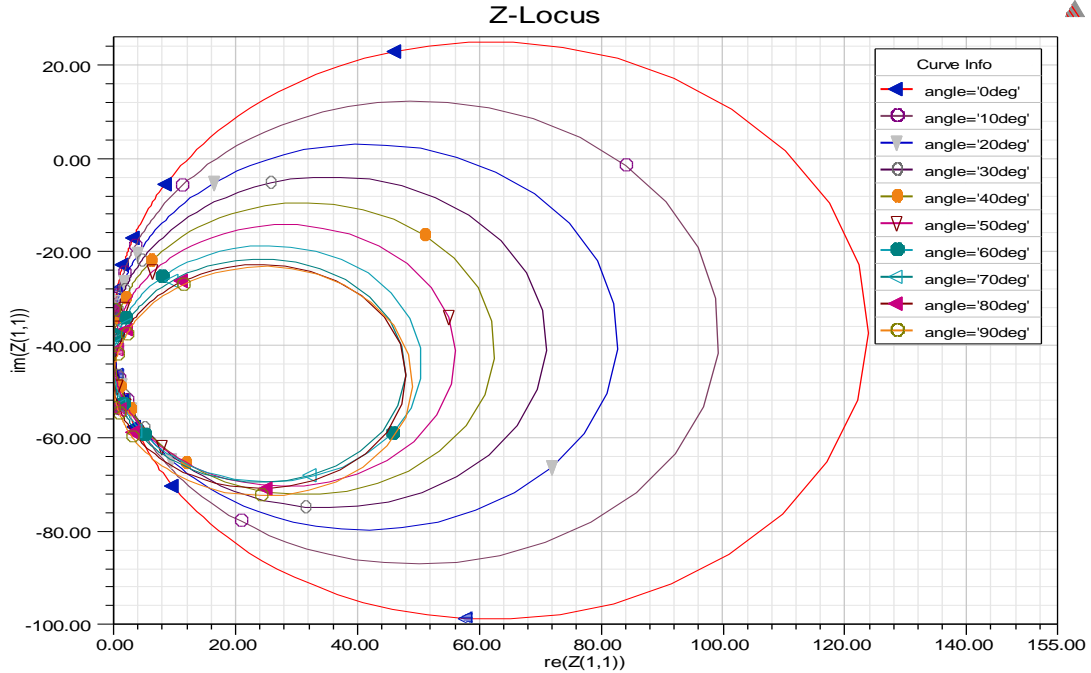
Figure 3.7 Simulated Z-plane locus

3.2.3.2 Circuit model

Applying the proposed procedure on an angular tuned resonator, we will commence when the angle equals 0°. From HFSS, we can see that the coupling is capacitive.

 Finding the coupling element (C_c)

Following the procedure stated previously, we will find C_c by knowing Z_{in} and the Z-locus diagram of Z_u. Figure 3.8 shows the ADS schematic of the two circuits used as a way to obtain the value of C_c. The unloaded input impedance (Z_u) is equal to the input impedance of the first circuit (Z_{in}) subtracted by the input impedance of the second circuit (Z_c).The "S1P" box in the figure represents the loaded resonator at an angle equal to 0°, simulated by the EM simulator.
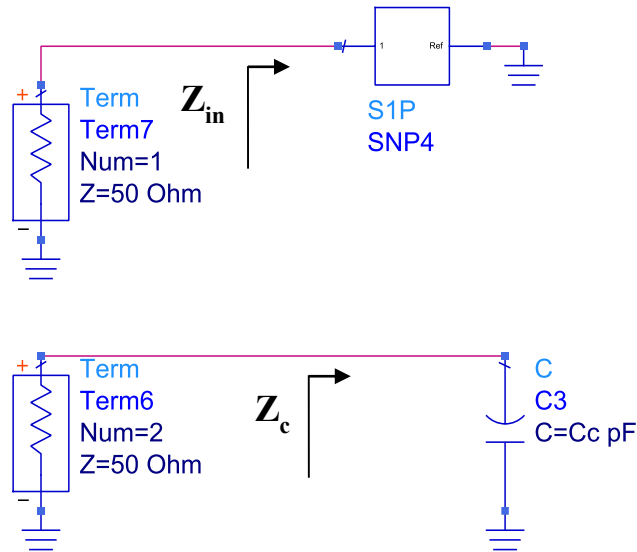
Figure 3.8 Finding the coupling capacitor (C$_c$)

The next step is to change the C$_c$ to get a symmetric Z-plane locus performance for Z$_u$. The value of C$_c$ is found to be **1.152pF**. Figure 3.9 shows the Z-plane locus of Z$_u$ at the C$_c$ value stated.

After obtaining the coupling capacitor, it is normal to notice a shift in center frequency due to the coupling. The loaded center frequency (f$_L$) is 3.7538 GHz, while unloaded (f$_o$) it is 3.7542 GHz. The unloaded Q is calculated to be 5538.887.

Eqn Zu=Z(1,1)-Z(2,2)
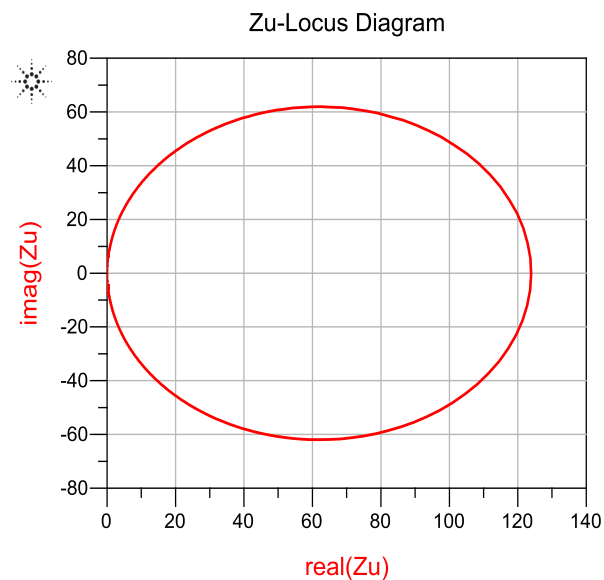
Figure 3.9 Z-plane locus of unloaded input impedance Z$_u$ (at C$_c$=1.152pF)

Finding tank circuit parameters

To identify a tank circuit, we need to find R_o, C_o and L_o.

$$R_o = Max\big(Real(Z_{in})\big) = \mathbf{123.862}\ \boldsymbol{\Omega}$$

For parallel resonance using Equations (3.4) and (3.5), we can find C_o and L_o.

Therefore,

$$C_o = \mathbf{1.895}\ \boldsymbol{nF}$$

$$L_o = \mathbf{0.94802}\ \boldsymbol{pH}$$

Figure 3.10 shows two circuits, the first one representing the EM model, and the second one representing the equivalent circuit model. Both are at an angle equal to 0°.   Table 3.1 shows the values of all four parameters needed to characterize the model.

Table 3.1 Equivalent circuit parameters

Parameter	Final values for angle=0°
R_o	123.862 Ω
L_o	0.94802 pH
C_o	1.895 nF
C_c	1.152 pF
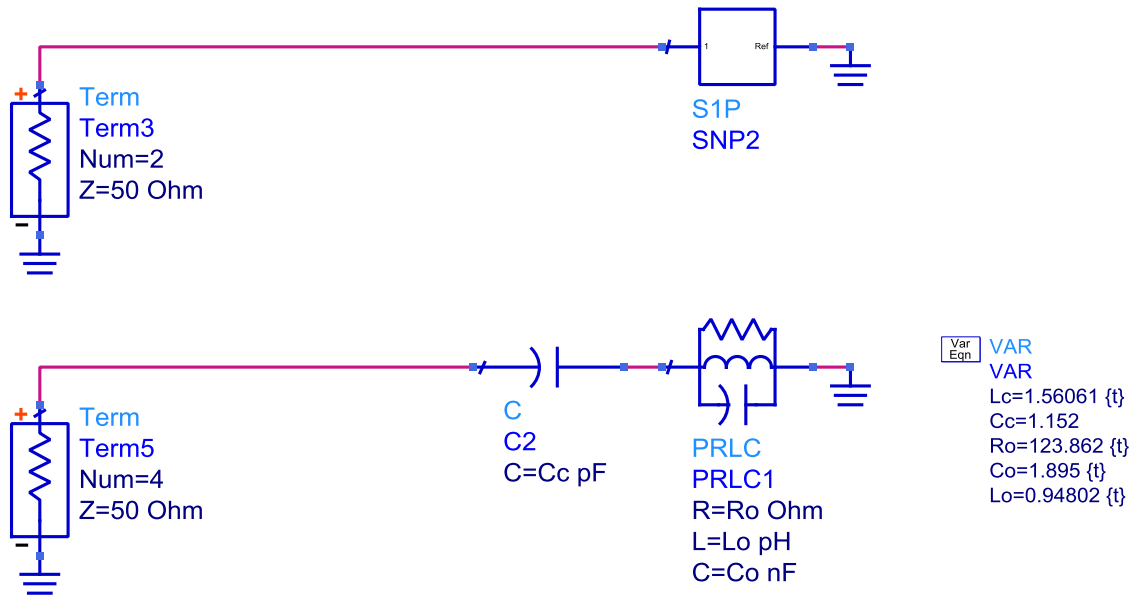
Figure 3.10 EM resonator model compared to the equivalent circuit resonator model
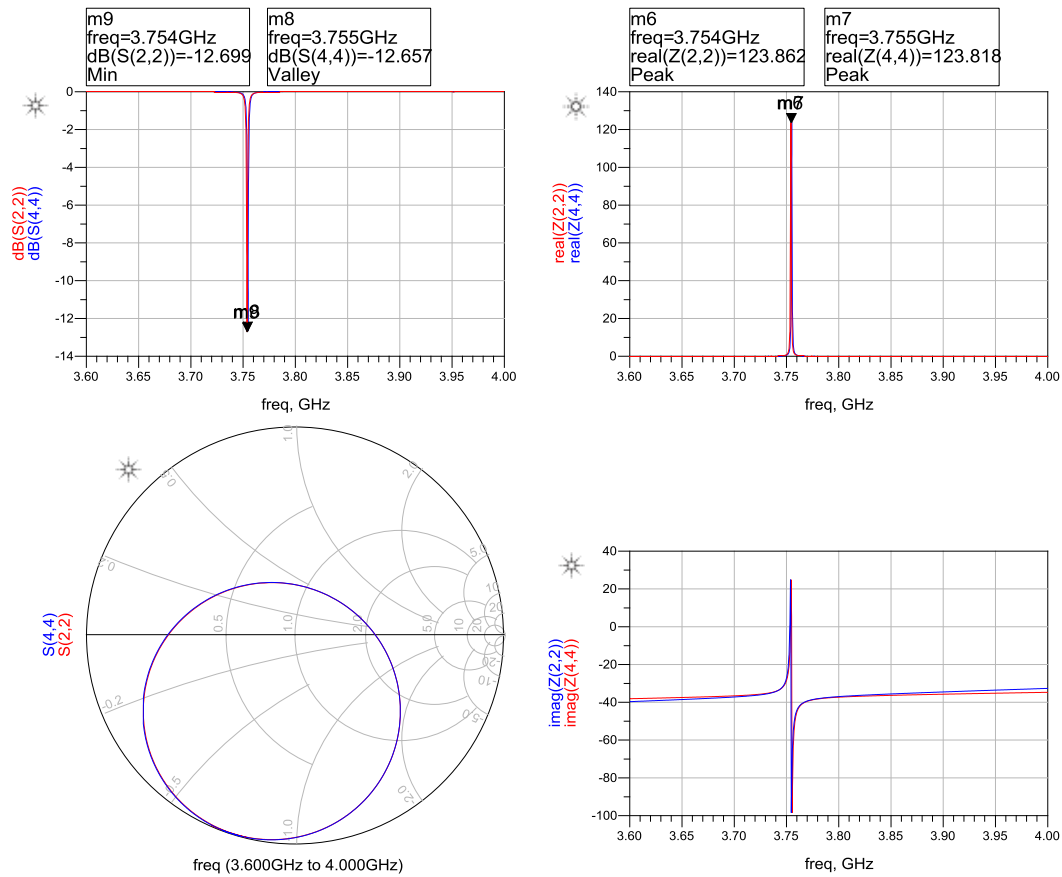
Figure 3.11 EM model versus circuit model for the case study example at angle=0°

Figure 3.11 shows the exact match for both models in input reflection coefficient magnitude as well as smith chart. Both real and imaginary Z_{in} fit very well. The red curve represents the EM model's performance and the blue represents the circuit model's.

Allowing for tunability (R_{tune} and/or C_{tune} and/or L_{tune})

- Circuit #1: Connecting R_{tune} and C_{tune}

To allow the circuit model to describe the tunability of the resonator, a new varactor is added C_{tune} ("Cchange" in the ADS model) to model the frequency shift. Also, after noticing that the resistance value is changing from one state to another, a new resistor R_{tune} ("Rchange1" in the ADS model) is added to track these changes. Figure 3.12 shows the equivalent circuit after adding the capacitance and resistance. Choosing a capacitance to model the frequency shift is the result of noticing that the EM model's center frequency is tuned by changing the overlap area between tuning element and post, which in turn changes the capacitance.

22
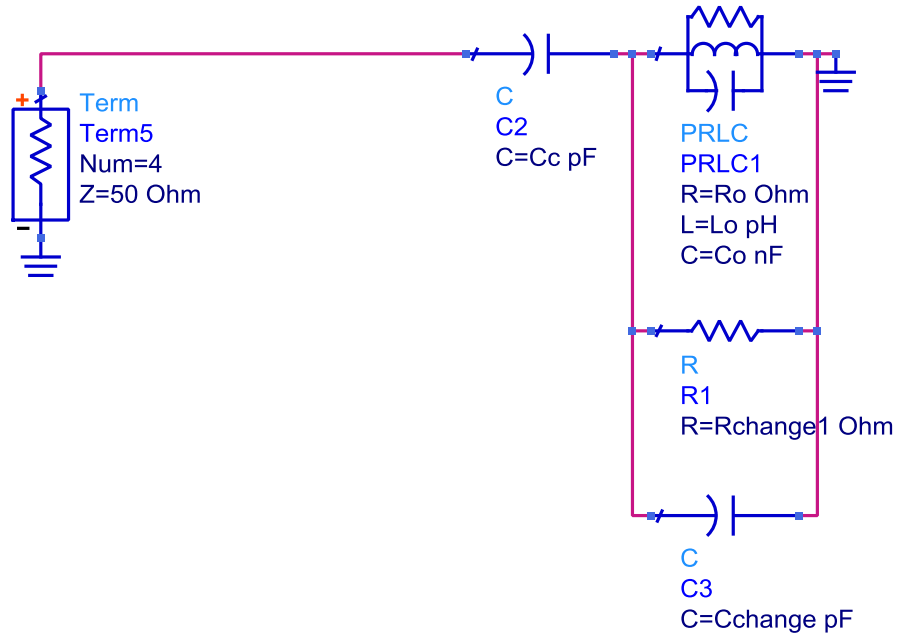
Figure 3.12 Equivalent circuit #1 (adding R$_{tune}$ and C$_{tune}$)

The values of R$_o$, C$_o$ and L$_o$ are kept as in Table 3.1. "Cc", "Cchange" and "Rchange" are the parameters to be changed to track the resonator's tuning behavior.

The matching is done in three steps, as follows:

1- Getting "Cc".
2- Tuning "Cchange" to match the frequency shift.
3- Tuning "Rchange" to match the response.

Table 3.2 Parameter values to allow for tuning

	0°	10°	20°	30°	40°	50°	60°	70°	80°	90°
R_{change} (Ω)	-	504.6	250.06	166.89	126.59	102.54	85.39	78.071	78.485	81.509
C_{change} (pF)	-	23.81	76.6	139.66	216.67	308.67	407.67	503.5	587	655
L_c (nH)	1.5606	1.5862	1.6393	1.7326	1.8231	1.9334	2.0536	2.1668	2.2671	2.3493
C_c (pF)	1.152	1.147	1.1409	1.1093	1.0983	1.0803	1.0633	1.0493	1.0383	1.0293

The circuit #1 model closely matches the HFSS model in the center frequency, smith chart and Z$_{in}$, but in terms of Γ$_{in}$ notch sharpness, they are different. Changing the capacitance is not enough to fully match the sharpness of Γ$_{in}$, which made a difference in the Q value of both. Table 3.2 shows the differences in Q_o between circuit #1 and the EM model.

Table 3.3 Comparing Q_o for circuit #1 model and EM model

Angle	Circuit #1 $Q_o = \dfrac{R_T}{2\pi f_o L_o}$	EM MODEL Q_o
0°	5539.486861	5538.8872
10°	**4474.54392**	**5517.611**
20°	**3777.895234**	**5468.1389**
30°	**3294.197043**	**5517.1395**
40°	**2954.72803**	**5623.0646**
50°	**2704.426111**	**5649.7518**
60°	**2491.708488**	**5577.2746**
70°	**2408.806369**	**5569.8841**
80°	**2458.540305**	**5607.0753**
90°	**2549.949363**	**5693.7563**

- Circuit #2: Connecting R_{tune}, C_{tune} and L_{tune}

To fix this issue, "Lchange" is connected as in Figure 3.13 and the process is repeated to get the equivalent circuit parameters.
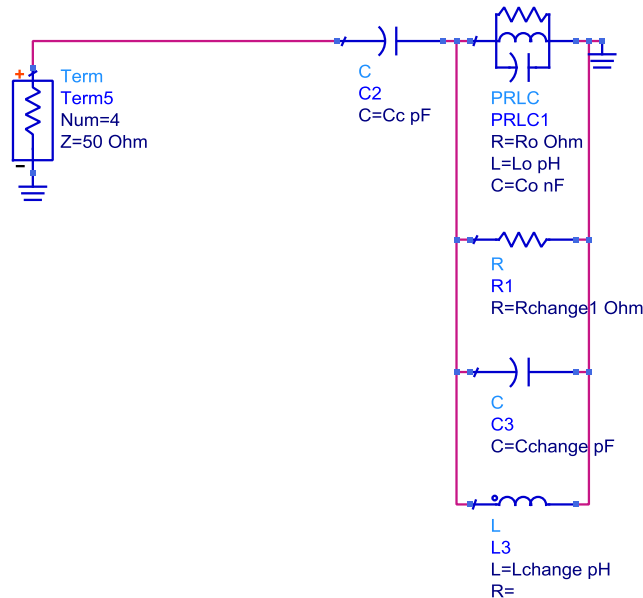
Figure 3.13 Equivalent circuit #2 (adding R_{tune}, C_{tune} and L_{tune})

The values of R_o, C_o and L_o are maintained, as in Table 3.4. "Cc", "Cchange", "Rchange" and "Lchange" are the parameters to be changed to track the tuning behavior of the resonator. Hence, the circuit model is now in exact agreement with the EM model.

Table 3.4 Parameter values to allow for tuning

	0°	10°	20°	30°	40°	50°	60°	70°	80°	90°
R_{change} (Ω)	-	504.6	250.1	166.9	126.6	102.5	85.39	78.07	78.49	81.51
C_{change} (pF)	0	0.47	0.958	1.513	2.122	2.707	3.261	3.651	3.766	3.8
L_{change} (pH)	inf	4.067	2.119	1.405	1.05	0.87	0.766	0.722	0.74	0.77
C_c (pF)	1.15	1.147	1.141	1.109	1.098	1.080	1.063	1.049	1.038	1.029
Q Circuit Model	5539	5518	5468	5517	5623	5650	5577	5570	5607	5694

Figure 3.14 shows the change of "Cchange" and "Lchange" versus center frequency. Figure 3.15 shows the change of the coupling capacitor "Cc". As can be seen, the change is quite insignificant and can easily be predicted from the Z-plane locus performance of the EM model in Figure 3.7. The shift is almost the same for all circles.
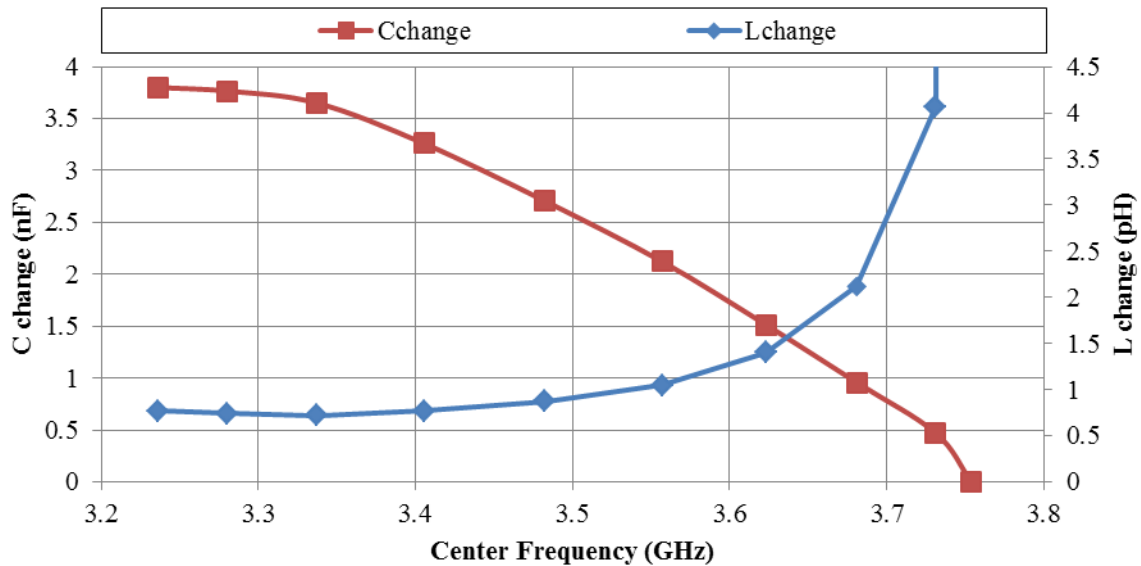
Figure 3.14 Cchange and Lchange versus frequency
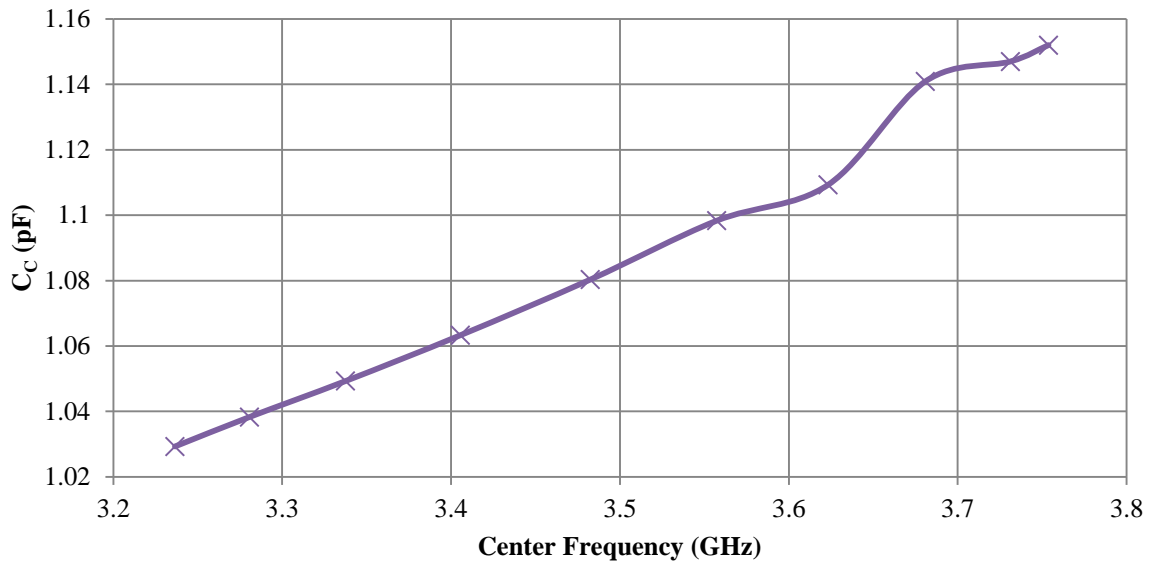
Figure 3.15 Cc versus frequency

3.2.4 Discussion

The circuit model discussed previously matches the resonator performance and tunability very well. The same applies to all tank circuit models discussed in the literature [28]. The drawback for these models is that they do not take other RF resonance modes into consideration and, more importantly, do not relate to the EM physical resonator. For example, when tuning the physical resonator, we expected only the capacitance to change significantly "Cchange". However, while working on the model, we found out that the inductance also had to change to keep track of the Q performance. The "Cchange" should be connected; otherwise, it might give the same effect as the EM physical resonator.

To overcome this problem, a model that can account for other modes and also has a one-to-one (or node-to-node) analogy with a physical EM model is needed.

3.3 The Node-to-node Modeling Technique

3.3.1 Equivalent circuit model explanation

In this approach, we will try to let the circuit model match the 3D model, following the node-to-node technique. Figure 3.16 shows the coaxial cavity short-circuited from both ends. The coaxial SMA is connected at the walls of the cavity to couple the microwave energy inside the resonator. To describe this 3D resonator using the node-to-node technique, we will begin by identifying the nodes.
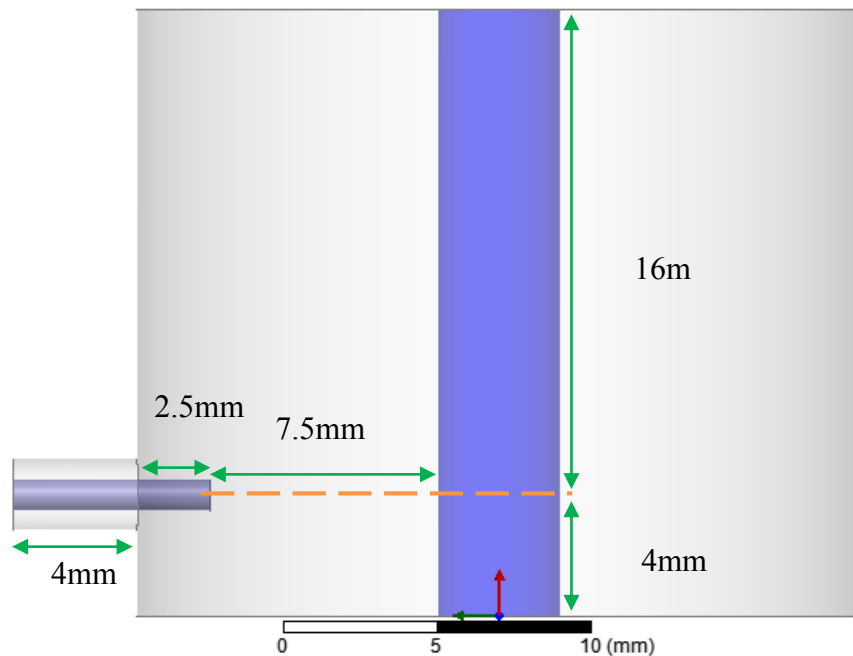
Figure 3.16 Coaxial cavity short-circuited from both sides

Figure 3.17 shows the nodes annotated on top of the 3D model. We have five nodes here, in addition to the ground. (The cavity walls and the outer conductor of the input SMA are considered as ground.) We will use the coaxial transmission line circuit model in ADS as well as lumped components to model the sections between each node. For instance, between nodes 1 and 2, we have a coaxial line with known inner and outer radii, length and dielectric, which can be easily modeled in ADS. We will use model nodes 2 to 3 as an inductance to model the inner conductor extension and then a capacitance to model the air gap between the tip of the inner conductor and the vertical post. We will also add a capacitance to the ground. At node 3, we will assume that we have a T- junction, the first end coming from the input, the second going upward, and the third going downward. From

27

node 3 to node 4 (as well as for node 5), we have a coaxial transmission line with known parameters going to the bottom plate (top) and then to ground. The plate can be modeled as an ideal short circuit or, more accurately, a resistance, as we will show later.
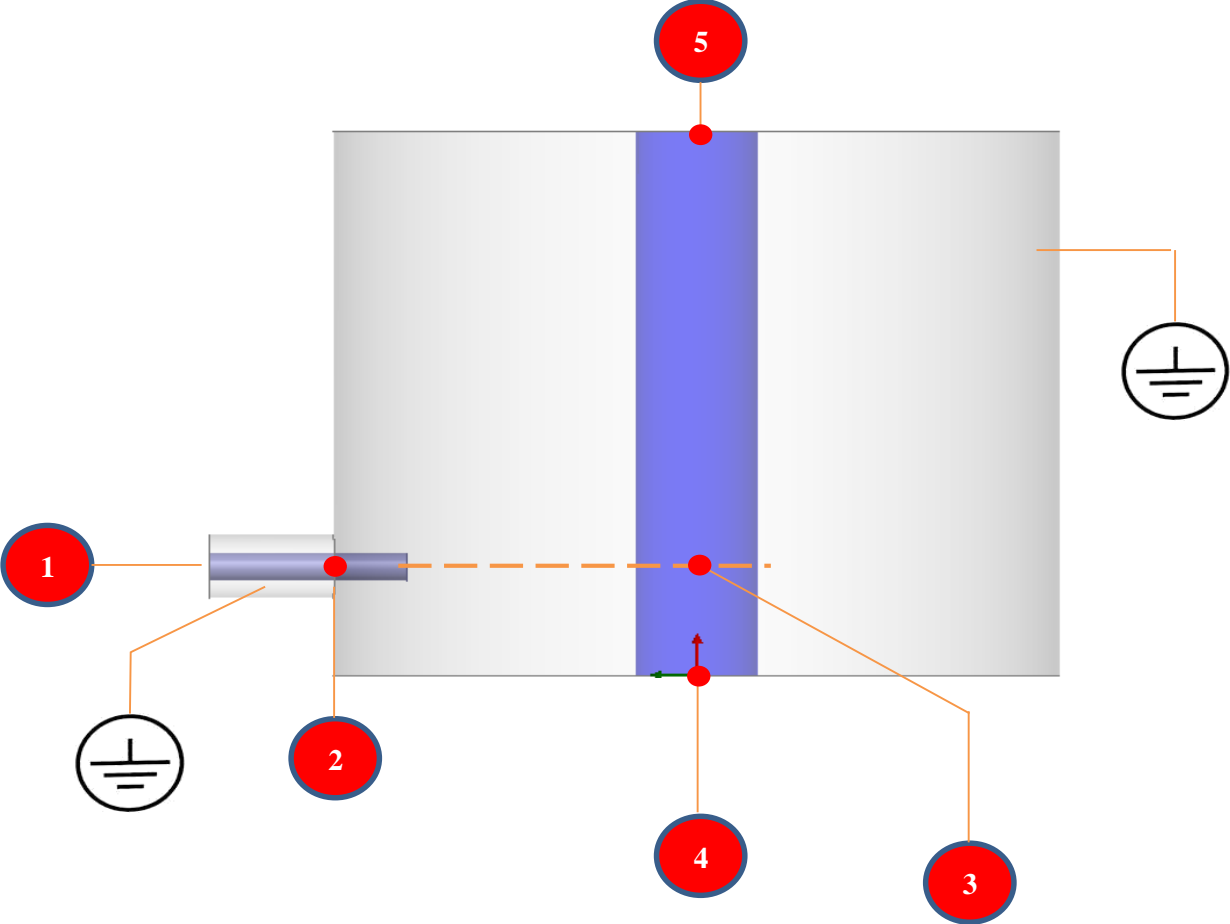
Figure 3.17 Coaxial cavity short-circuited from both sides with all nodes
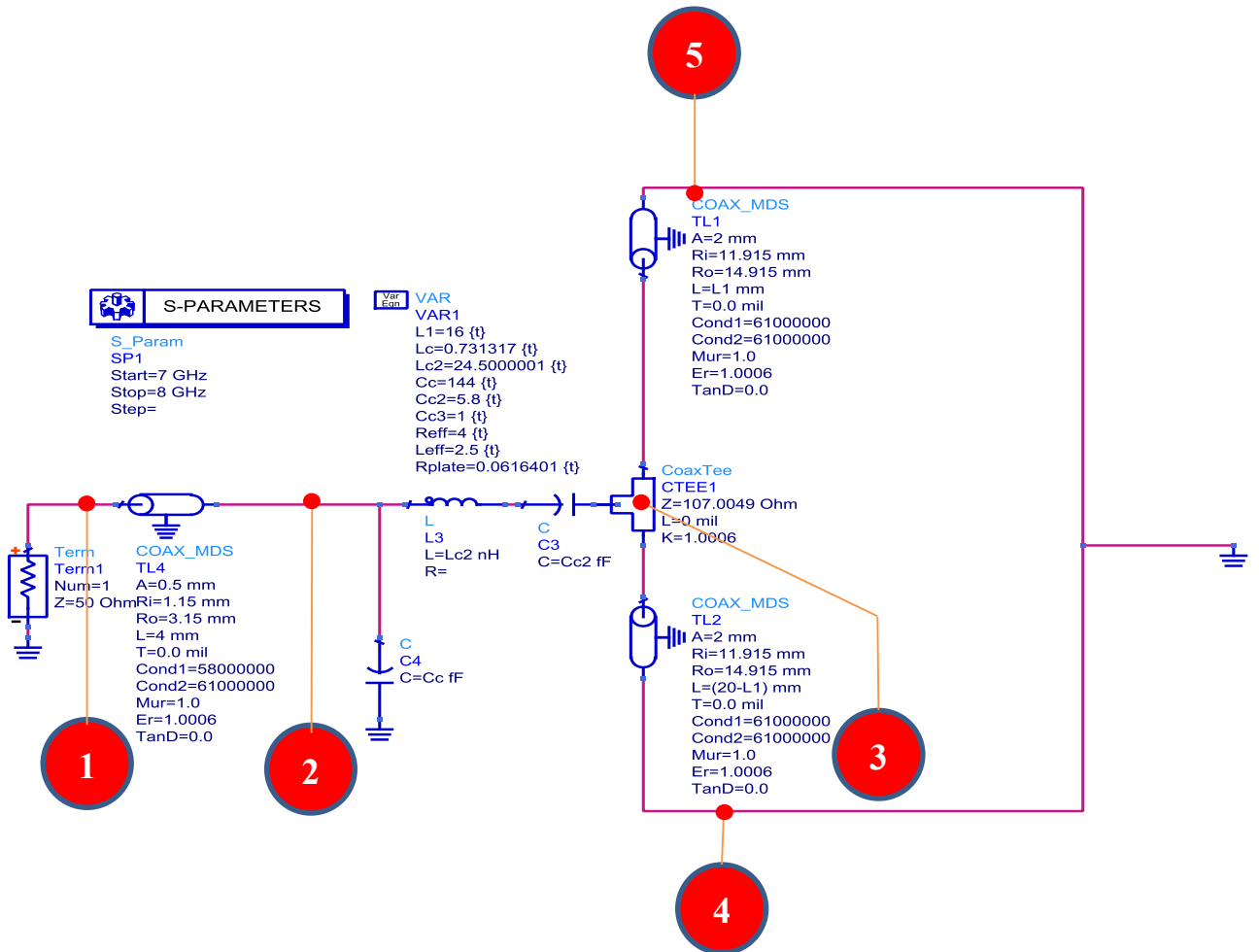
Figure 3.18 Equivalent circuit model following node-to-node technique
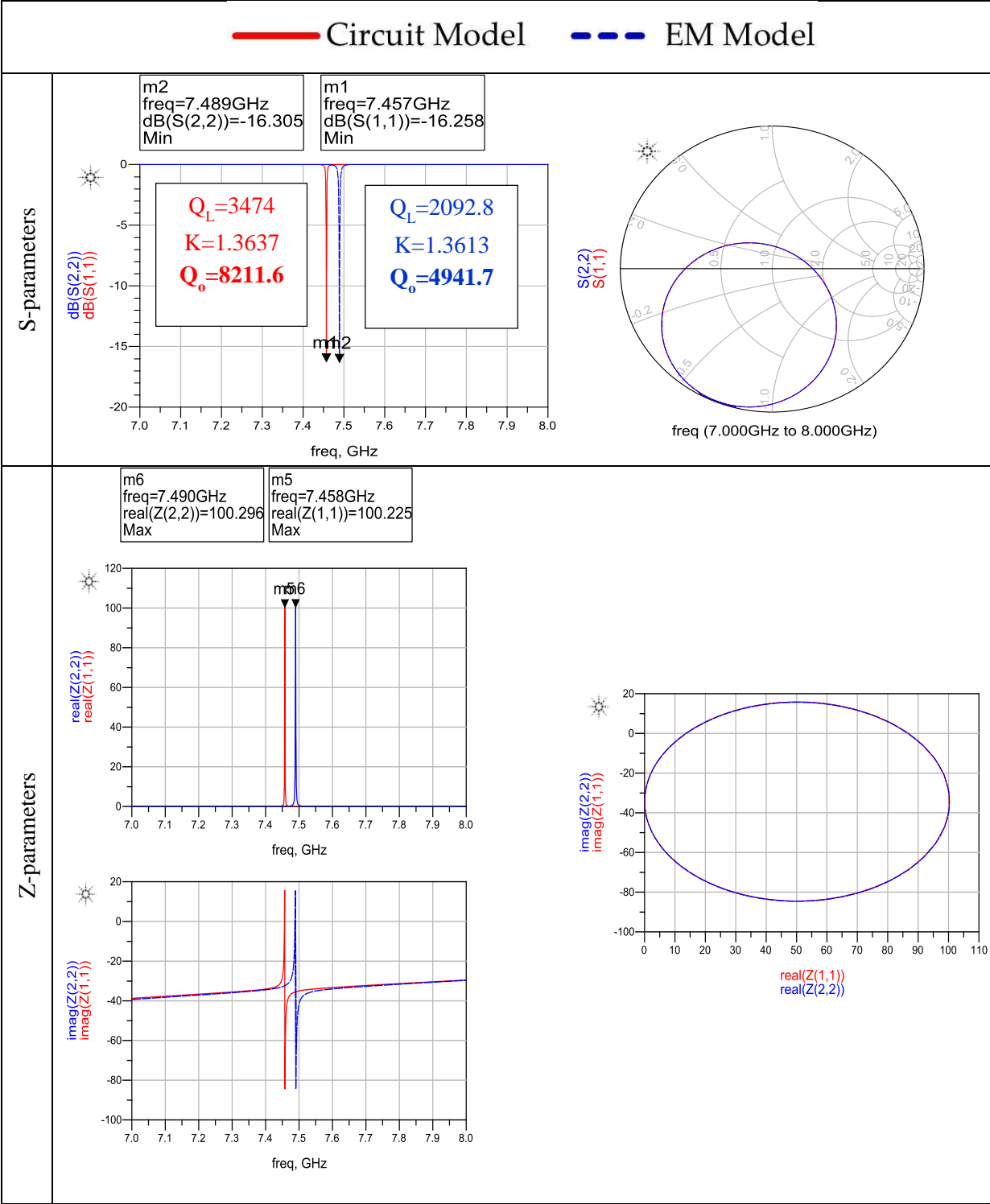
Figure 3.19 A comparison between the EM model's and circuit model's performance

Figure 3.18 shows the proposed equivalent circuit. The coaxial transmission line model is used several times to describe the input SMA connector as well as the resonator itself. The values of the lumped components are tuned to let the model performance fit the EM performance. A comparison between both performances is presented in Figure 3.18. Despite bearing some slight differences in center frequency and Q, the similarities in phase, shape and performance are remarkable.

To match the center frequency perfectly, one can add more lumped components. To fix the Q difference, we add the effect associated with grounding both ends of the transmission line. Specifically, the ground was assumed to be perfect, but practically the transmission line is grounded by top and bottom plates that connect the inner conductor to the outer. This can be presented by a resistance "Rplate" connecting each end of the transmission line to the ground. The equivalent circuit will then be as shown in Figure 3.20.
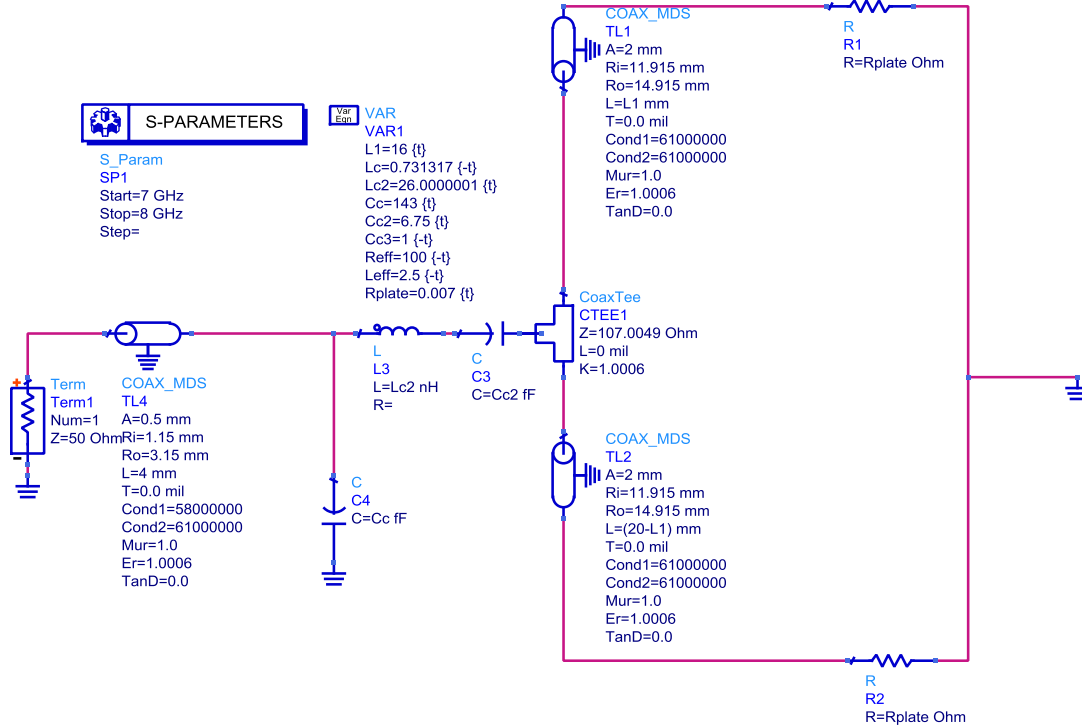
Figure 3.20 Equivalent circuit model after adding the effect of plate resistance

31
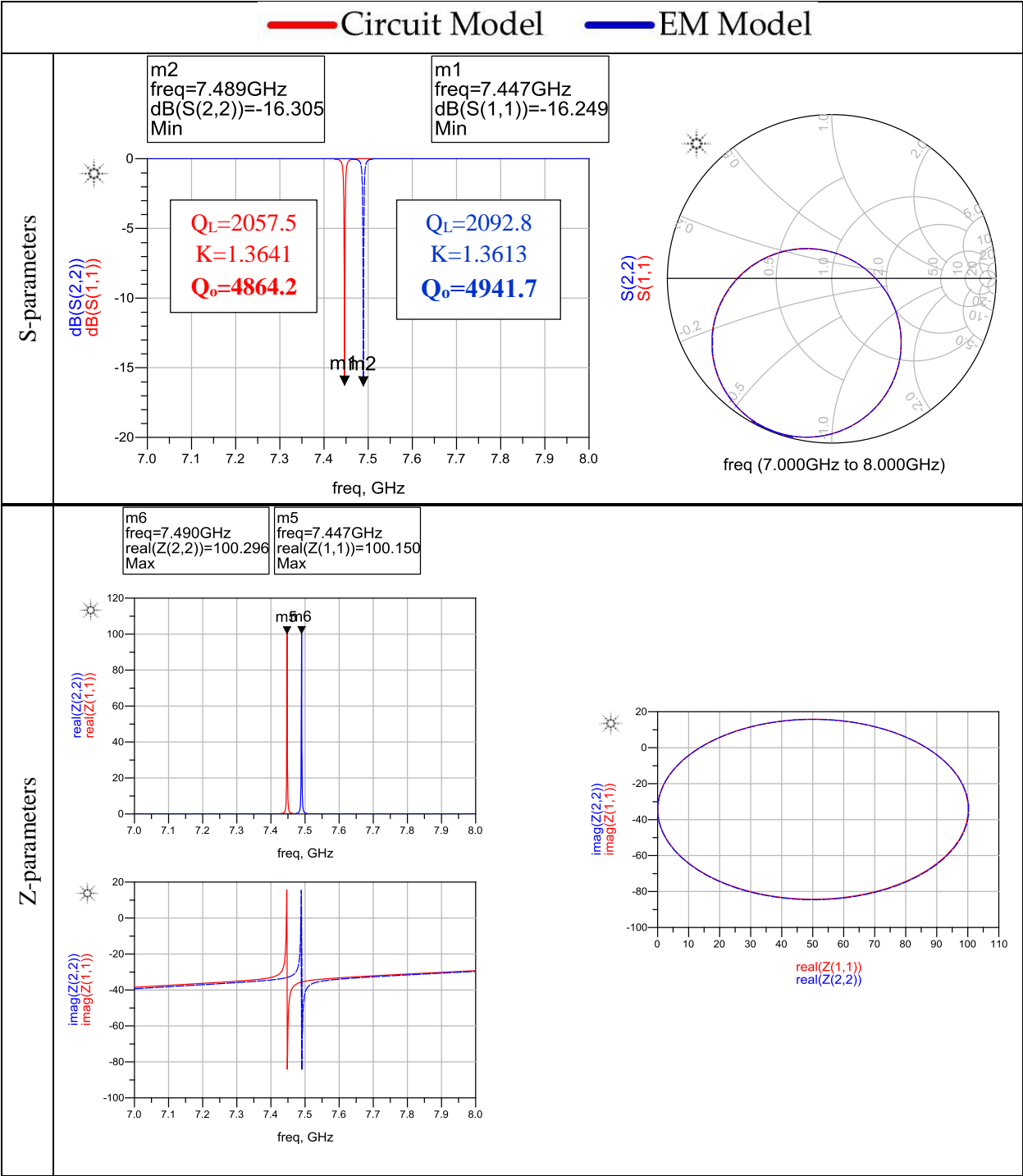
Figure 3.21 A comparison between the EM model's and circuit model's performance after adding the effect of plate resistance

Figure 3.21 shows a comparison between the performance of the circuit model and the EM model after adding the effect of plate resistance. Table 3.5 indicates that there is a very good match between the two models in terms of center frequency and Q factor. We can note a small shift of 42 MHz in center frequency between the EM model and the circuit model, which is caused by many factors, such as the coaxial transmission line model used and/or the simplified coupling circuit used. To match the center frequency perfectly, one can add more lumped components.

Table 3.5 A comparison between the EM model and circuit model

	f_o	Q_o
EM model	7.489GHz	4941.7
Circuit model	7.447GHz	4864.2

Thus far, the equivalent circuit model is performing similarly to the EM model. To validate the model even more, we are going to carry out a change in the EM model. We will do the same in the circuit model and then check to see how well the two changed models match each other.

3.3.2 Equivalent circuit model validation

The 3D model above consists of a combline resonator short-circuited from both sides. In an attempt to validate the circuit model, we will change the EM model by having a gap at one end of the resonator while the other end will be kept as a short circuit, as shown in Figure 3.22. This can be translated in the circuit model into a capacitance at the end where we have a gap.
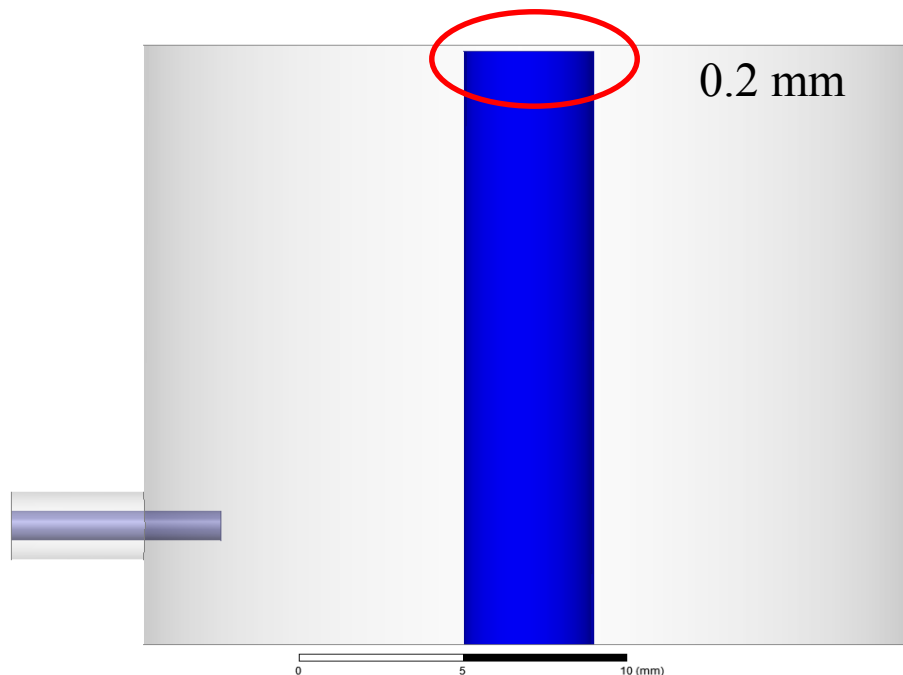
0.2 mm

Figure 3.22 A 3D resonator model after adding a 0.2mm gap at the top end

As mentioned previously, the gap will be modeled as a capacitor. The capacitor will be connected between node 5 and the wall (plate resistance to ground). However, we need to find the capacitance value associated by the gap. For this, we will use the parallel plate capacitance formula to obtain an approximation of the capacitance value.

$$C = \frac{\varepsilon_o A}{d} = \frac{8.8541 \times 10^{-12} \times \pi \times (2 \times 10^{-3})^2}{0.4 \times 10^{-3}} = 556\ fF$$

Having a 0.2 mm gap in the 3D model will allow a new mode to rise (~1.8GHz) in the EM simulation, as shown in Figure 3.23. At the same time, mode 2 is shifting upwards in frequency compared to the short-circuit case.

Eigenmode	Frequency (GHz)	Q
Mode 1	1.81434 +j 0.000293505	3090.81
Mode 2	7.91885 +j 0.000825524	4796.26

Figure 3.23 EM simulation (eigen mode) for the model with a gap at the top end

After connecting the 556 fF capacitance into the circuit model, we end up by having the circuit shown in Figure 3.24.
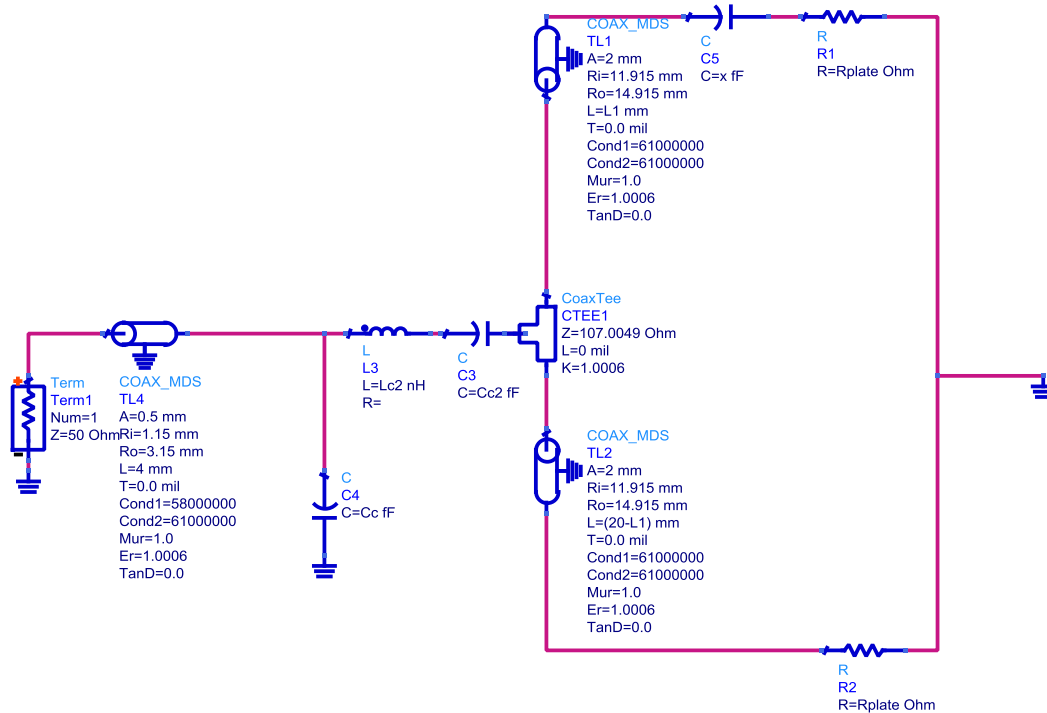
Figure 3.24 Circuit model after connecting the capacitance
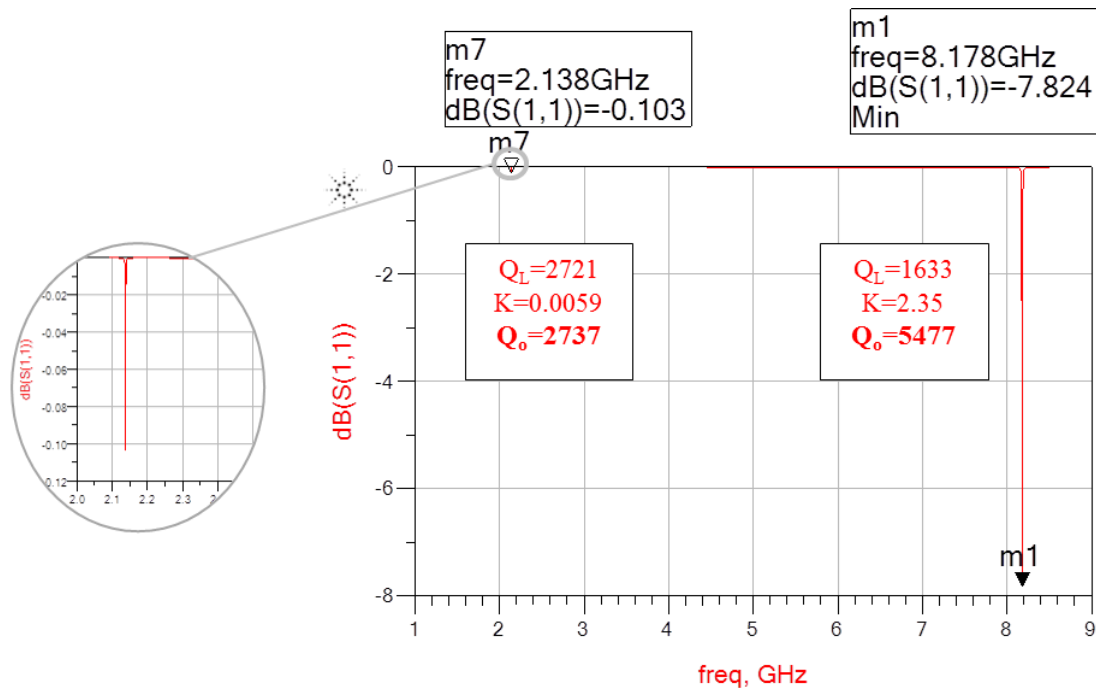
Figure 3.25 Γ_{in} **of the circuit model after adding capacitance at the top end**

Figure 3.25 shows two modes: the first one is at 2.1GHz, and the second one is at 8.17GHz. These results provide confirmatory evidence that we can trust the circuit model to give us a very good estimate on how the resonator performs. Of course, if we adjust the capacitance value and the coupling circuit, we might get more accurate results. The point here, however, is that without spending time to fine-tune the coupling circuit and get an accurate capacitance value, we can obtain very satisfactory insight about the modes' center frequencies and *Q*-factor.

3.3.3 Applications

3.3.3.1 Center frequency and *Q*-factor changes due to ideal varactor

The goal of this section is to obtain an equivalent circuit model of a coaxial resonator that is short-circuited at one end while the other end is connected to an ideal varactor. The ideal varactor is connected to a substrate and couples to the coaxial resonator by two vias, one of which is connected to the post and the other of which is connected to the resonator walls (ground). Figure 3.26 shows the 3D EM model for the coaxial resonator.

Ideal Varactor

Via to gnd

Via to the post
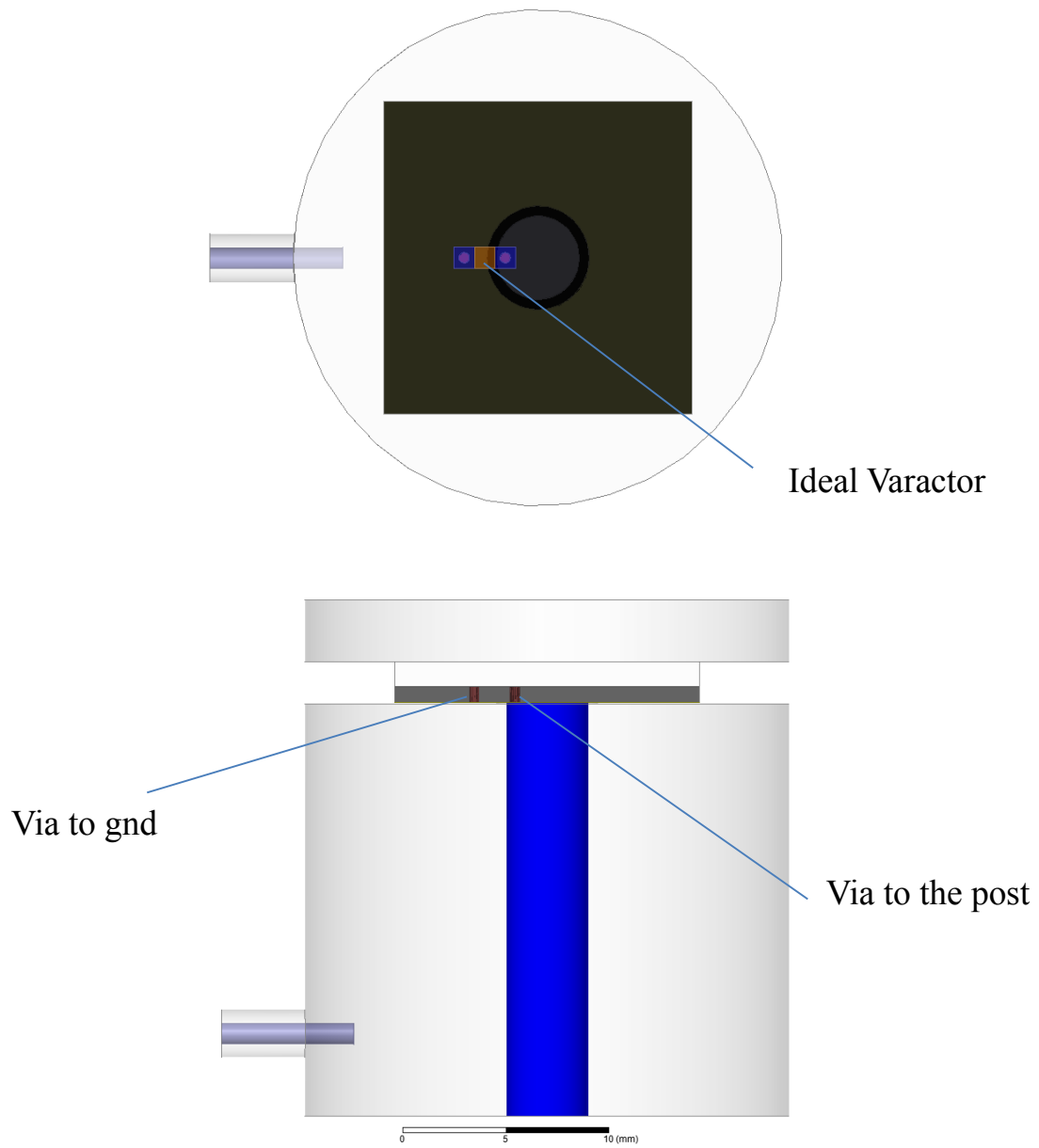
Figure 3.26 Different views for the EM model of a coaxial resonator connected to an ideal varactor at the top end

In order to achieve a circuit model for the actual model shown in Figure 3.26, we will use a step-by-step approach to get a better understanding of each element in the model (e.g., how and why it is connected the way it is).

The step-by-step procedure is as follows:

1- Short-circuit model
The first step is to get a circuit model that matches the resonator with the exact same size and is short-circuited at both ends.

2- Adding Substrate Effect
The next step is understanding how a substrate on top of the resonator affects the Q and f_o. Then, we add the substrate equivalent representation in the circuit model to match the EM simulations.

3- Final model with the varactor and vias
The final step is to add the varactor and vias to the EM model, which results in adding some other components that model vias and varactor to the circuit model. The goal is to allow the circuit model to keep track of the variations in Q and f_o that results in varying the capacitance of the varactor.

Short-circuit Model

Here, a similar modeling procedure to the one in section 3.3.1 is carried out, but for a different resonator height (22 mm instead of 20 mm). Figure 3.27 shows the equivalent circuit model. A comparison between the performance of the EM model and that of the circuit model is shown in Figure 3.28.
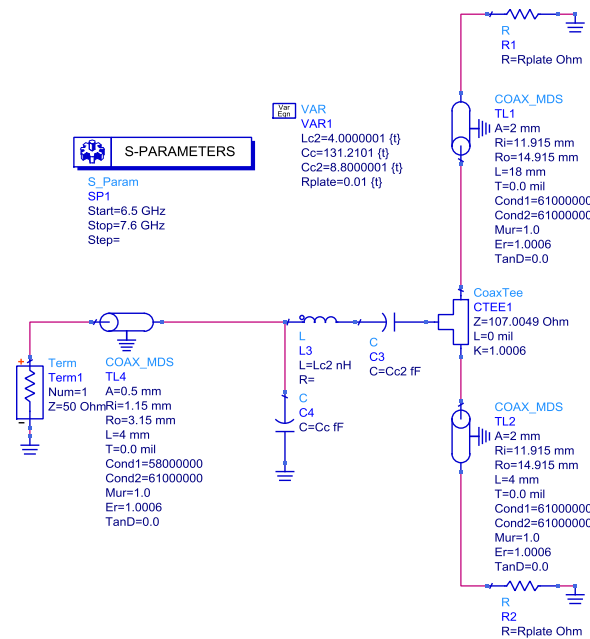
Figure 3.27 Equivalent circuit model for coaxial resonator short-circuited at both ends with a height of 22 mm

37
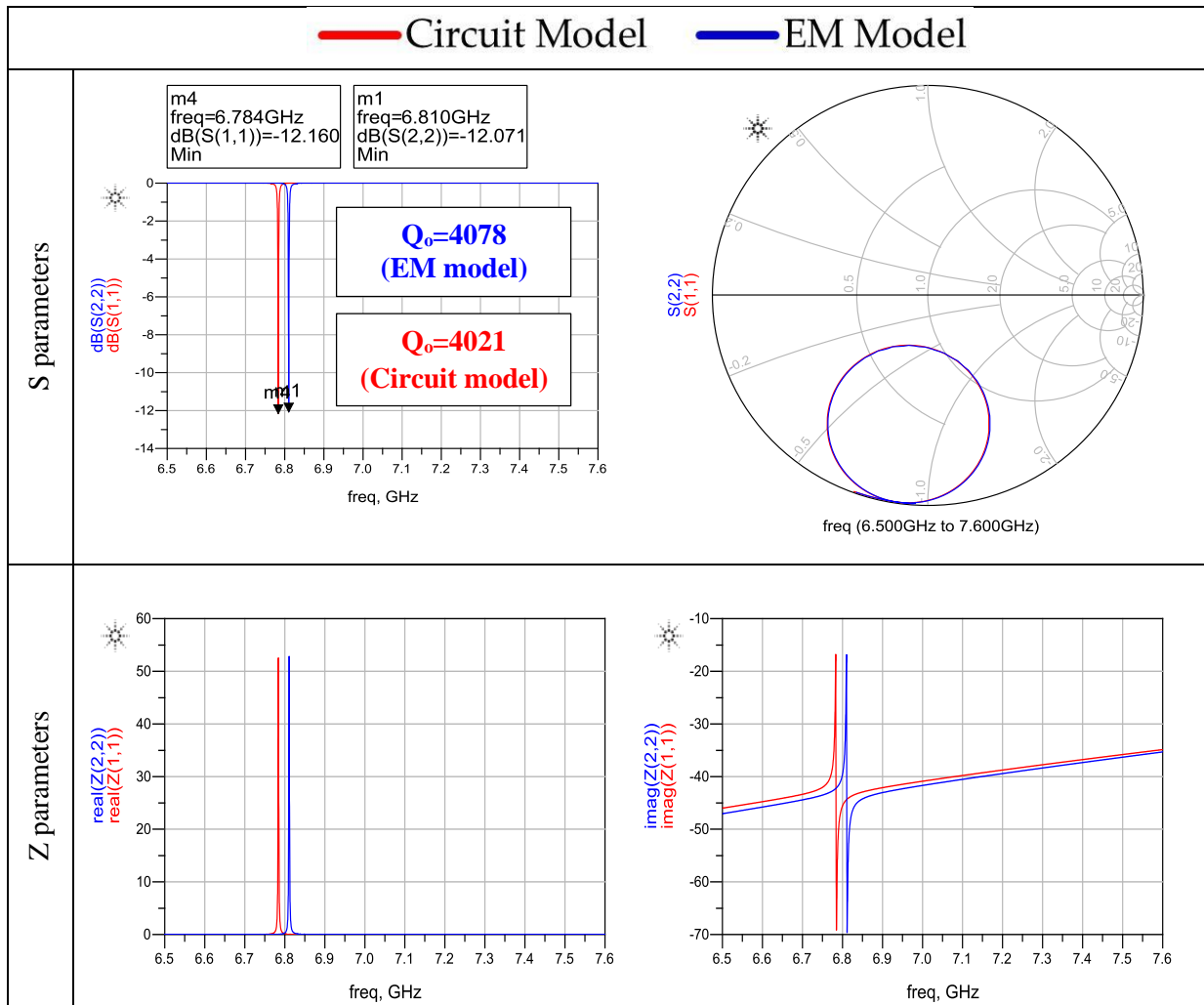
Figure 3.28 A comparison between an EM model's and a circuit model's performance

Adding the substrate effect

To understand the substrate effect, a couple of EM simulations are done. We will start with the same resonator and leave the upper end unconnected to the ground. For the first simulation, we will leave room for the substrate but we will not put it. That is equivalent to having theoretically an air substrate. We will also keep the bottom gold layer, which represents the metallic traces printed on the bottom of the substrate.

For the second EM simulation, we will include an RT Duroid 5880 substrate with a thickness of 31 mils. This substrate has a relative dielectric constant of 2.2 and a loss tangent of 0.0009.

Frequency (GHz)	Q
7.85274 +j 0.00065...	6005.62
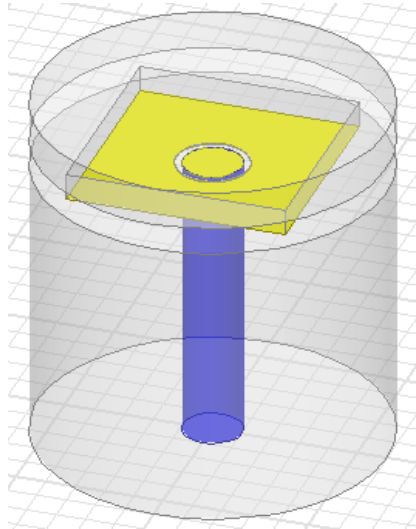
Figure 3.29 EM simulation results without the substrate

Frequency (GHz)	Q
7.65079 +j 0.00092...	4155.51
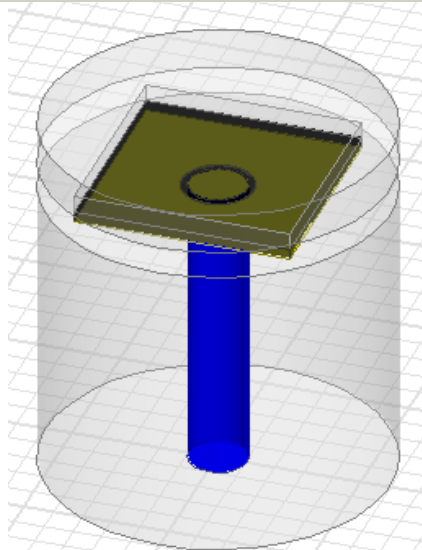
Figure 3.30 EM simulation results with the RT Duroid 5880 substrate

In comparing both simulations, we can conclude the following:

1- Although the top end of the resonator is left unconnected, this is not considered an open circuit. Nevertheless, there might somehow be a path to the ground, and this path varies when we use air or the RT Duroid 5880.

2- The change in center frequency means we have a capacitance in this path that changes because of the change of the relative permittivity from 1, in case of air, to 2.2, when the substrate is present.

3- The change in Q is modelled as a resistance in the path due to the change in the loss tangent (loss tangent=0.0009 in case of RT Duroid 5880).

The modification to be done on the equivalent model achieved in the last section is that we will omit the existing path to the ground in the top end of the resonator and replace it with a capacitance "Csubstrate" and a resistance "Rsubstrate" to the ground. The updated equivalent circuit is shown in Figure 3.31. Table 3.6 shows a comparison between the performance of the EM model and the circuit model.

Table 3.6 Comparison between EM model and circuit model after including the substrate effect

	f_o	Q_o
EM model	7.650GHz	4155.5
Circuit model	7.650GHz	4129.5
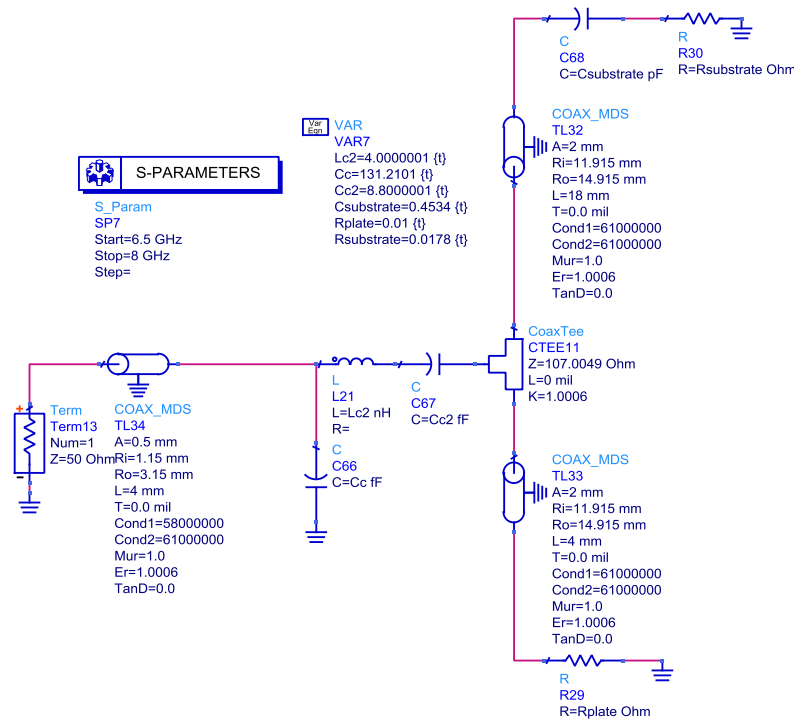
Figure 3.31 Updated equivalent circuit taking into consideration the substrate effect

<u>Final model (Adding varactor and vias)</u>

The final model includes the addition of the two vias, one to the post and the other to the ground. It also includes the connection of the ideal varactor between the two pads connected to the two vias. The EM simulation results showing the change in the center frequency and Q with the change in capacitance are shown in Table 3.7.

Table 3.7 EM simulation results showing the performance due to changes in capacitance

Capacitance (pF)	f_o (GHz)	Q_o
0.001	7.616	4159.1
0.1	7.437	3869.1
0.2	7.233	2961.7
0.3	7.005	2124
0.4	6.793	1608.8

Adding the vias and the varactor forms another path to the ground. The vias have a resistive and inductive effect, and the varactor has a capacitive effect. Furthermore, the presence of the vias might alter the capacitance inside the substrate and increase it slightly, which will need a fine tune for the value of "Csubstrate".

To make sure the circuit matches well for all capacitance values, we optimized the value of the added components to match Q and the center frequency for the initial, the median, and the final capacitance (0.001pf, 0.2pf and 0.4 pF, respectively). The resulting circuit is shown in Figure 3.32.

Figure 3.33 shows an excellent match between the EM model and the circuit model. Developing the model with the step-by-step procedure provided an excellent understanding of the circuit components and the possible ways to improve the performance. For example, we now have a very good idea about the effect of the substrate, how far it affects the performance, and how indispensable the usage of low loss substrates is for high-Q applications. Also, although while using an ideal varactor, a degradation in Q occurs, an interpretation for this occurrence can be given using the circuit model. Namely, the branch of the varactor becomes more and more dominant by increasing the capacitance value, and the via resistance's loss increases accordingly.

From a practical standpoint, the via technology provided by PCB companies for 2-layer substrates is not gold-filled but gold-plated. Gold-plated vias have stronger resistance, which results in more Q degradation. Also, the commercially available varactors have their own losses, which add extra resistance in the dominant path. All of these factors contribute to Q degradation. To get an idea of how well the commercial varactors perform, a simulation is presented in the next section using the circuit model.

L
L23
L=Lvia nH
R=

R
R33
R=Rvia Ohm

C
C72
C=0.001 pF

C
C69
C=Csubstrate pF

R
R31
R=Rsubstrate Ohm

VAR
VAR8
Lc2=4.0000001 {t}
Lvia=1.362 {t}
Cc=131.2101 {t}
Cc2=8.8000001 {t}
Csubstrate=0.4754 {t}
Rplate=0.01 {t}
Rsubstrate=0.0178 {t}
Rvia=0.114 {t}

S-PARAMETERS

S_Param
SP8
Start=6.5 GHz
Stop=8 GHz
Step=

COAX_MDS
TL37
A=2 mm
Ri=11.915 mm
Ro=14.915 mm
L=18 mm
T=0.0 mil
Cond1=61000000
Cond2=61000000
Mur=1.0
Er=1.0006
TanD=0.0

CoaxTee
CTEE12
Z=107.0049 Ohm
L=0 mil
K=1.0006

Term
Term14
Num=1
Z=50 Ohm

COAX_MDS
TL35
A=0.5 mm
Ri=1.15 mm
Ro=3.15 mm
L=4 mm
T=0.0 mil
Cond1=58000000
Cond2=61000000
Mur=1.0
Er=1.0006
TanD=0.0

L
L22
L=Lc2 nH
R=

C
C70
C=Cc2 fF

C
C71
C=Cc fF

COAX_MDS
TL36
A=2 mm
Ri=11.915 mm
Ro=14.915 mm
L=4 mm
T=0.0 mil
Cond1=61000000
Cond2=61000000
Mur=1.0
Er=1.0006
TanD=0.0

R
R32
R=Rplate Ohm

Figure 3.32 Final equivalent circuit model of a coaxial resonator connected to an ideal varactor at the top end, mounted on top of an RT Duroid 5880 substrate
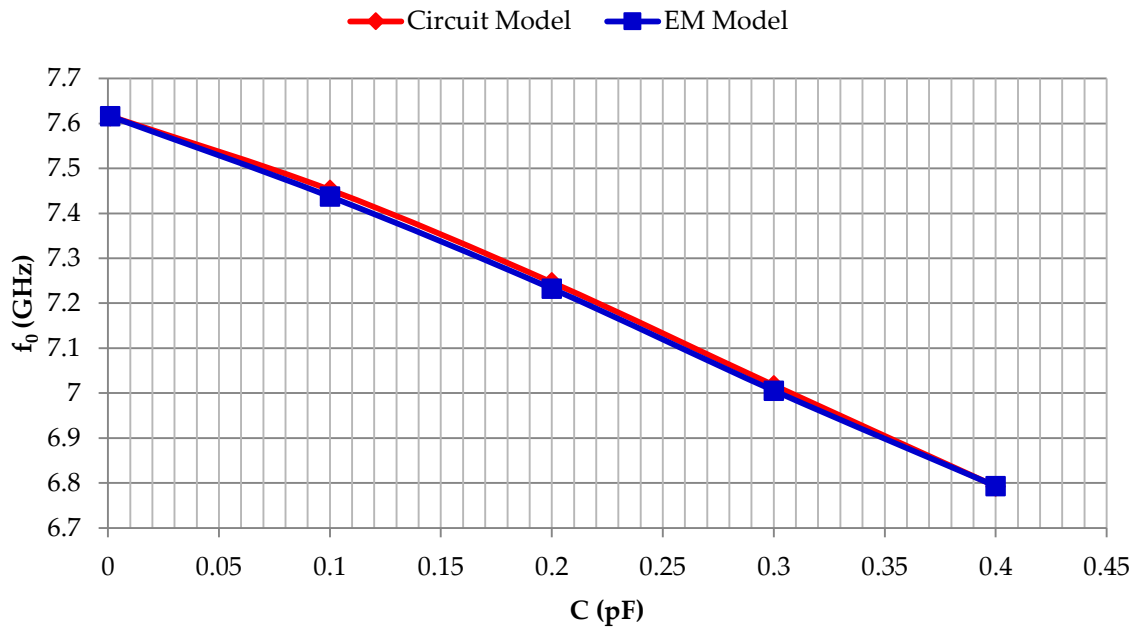
(a)
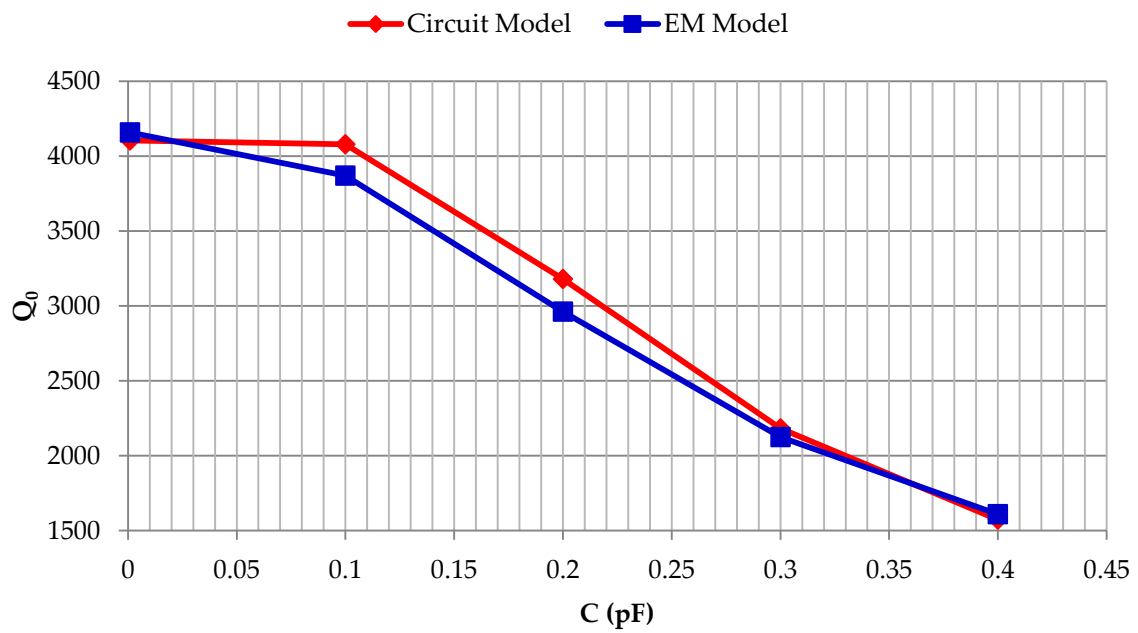
(b)

Figure 3.33 Comparison between circuit model and EM model performance:

(a) center frequency versus capacitance; (b) Q versus capacitance

43

Thus far, the equivalent circuit model is performing similarly to the EM model. To validate the model even more, we are going to carry out a change in the EM model. We will do the same in the circuit model and then check to see how well the two changed models match each other. The change is to add a resistor in series with the varactor. Figure 3.34
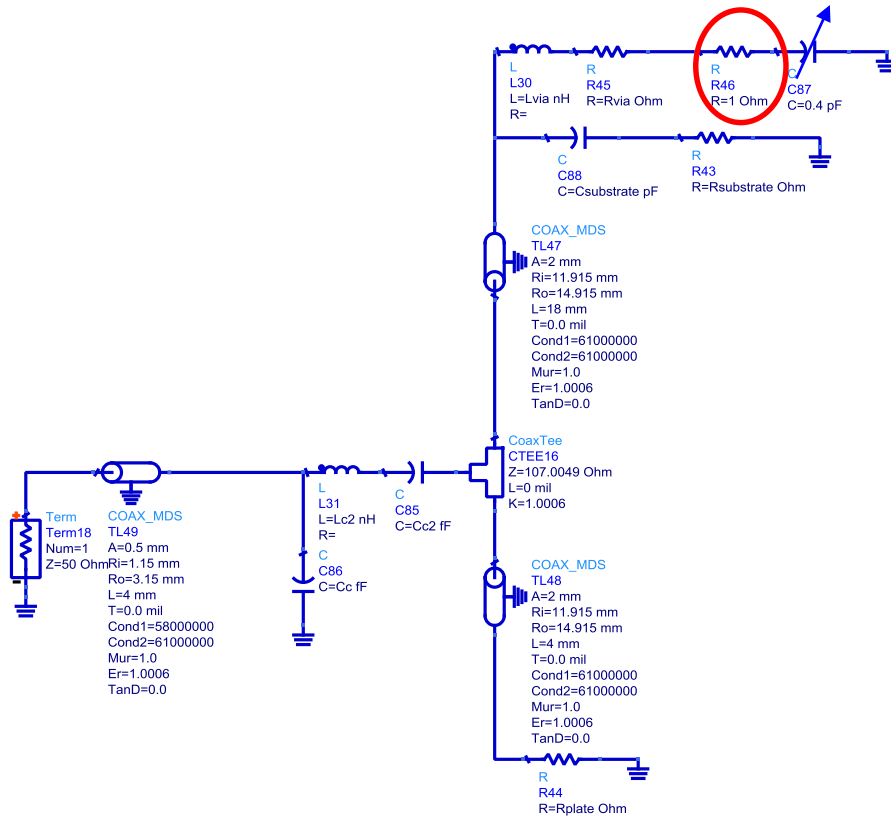
Figure 3.34 Equivalent circuit model after adding a resistance of 1 Ω in series with the varactor

Figure 3.35 shows an excellent match between the EM model and the circuit model. These results provide confirmatory evidence that we can trust the circuit model to give us a very good estimate on how the resonator performs. In the next section, we will connect this model to a commercial varactor model. This can be done now by virtue of the node-to-node technique.
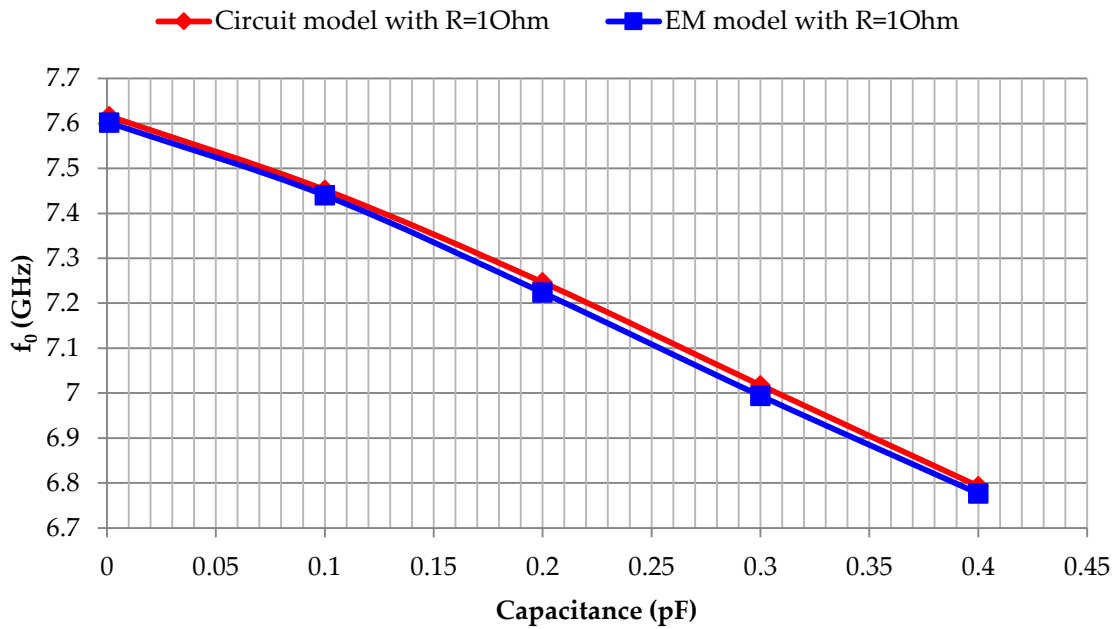
(a)
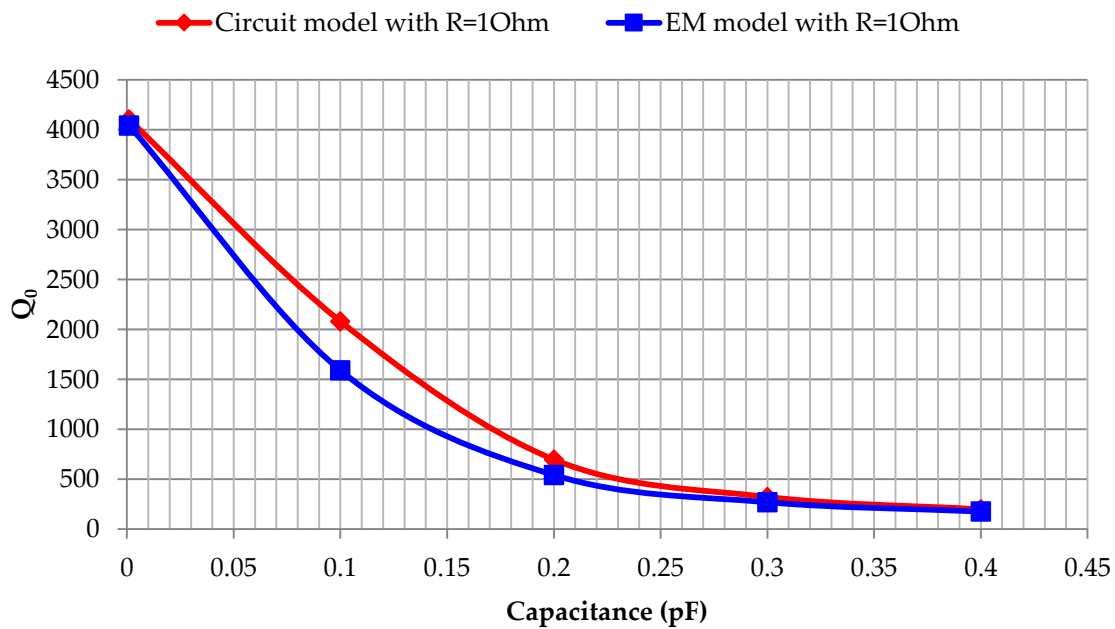
(b)

Figure 3.35 Comparison between circuit model and EM model performance after adding the resistance: (a) center frequency versus capacitance; (b) Q versus capacitance

45

3.3.3.2 Connecting commercial varactors

One of the main reasons this analysis was made is because HFSS as EM simulators do not allow S-parameter files to be connected within the EM simulator model. In other words, when we have a coaxial resonator that is short-circuited at one end while the other end is connected to a commercial varactor over a PCB to achieve tunability, this kind of simulation cannot be done in an EM simulator. An EM simulator allows only lumped components to be connected within the model.

The commercial varactor that we will use in the analysis is an MA-COM varactor. The model number is MA46603-134, which is one of the highest Q varactors (Q=6500 at 50MHz). The single port characterization of the varactor was done in the CIRFE Lab [30] and was characterized on a 25 mils alumina substrate with a relative dielectric constant of 9.9 and a loss tangent of 0.0001.
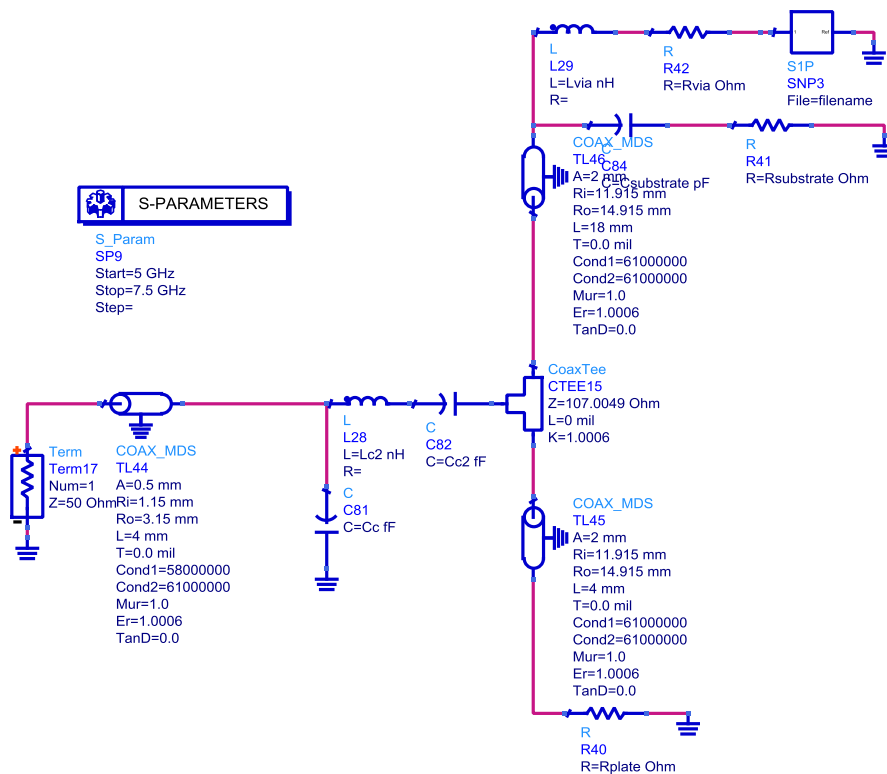
Figure 3.36 Commercial varactor connected to circuit model

The circuit is connected as in Figure 3.36. The S1P box in Figure 3.36 represents the varactor connected on top of the alumina substrate. The capacitance of the varactor changes by changing the DC bias of the varactor. Figure 3.37(a) shows a center frequency tuning range of 1.2GHz. The Q-factor variation is shown in Figure 3.37(b). The Q values reveal the huge effect that internal resistance has on performance.
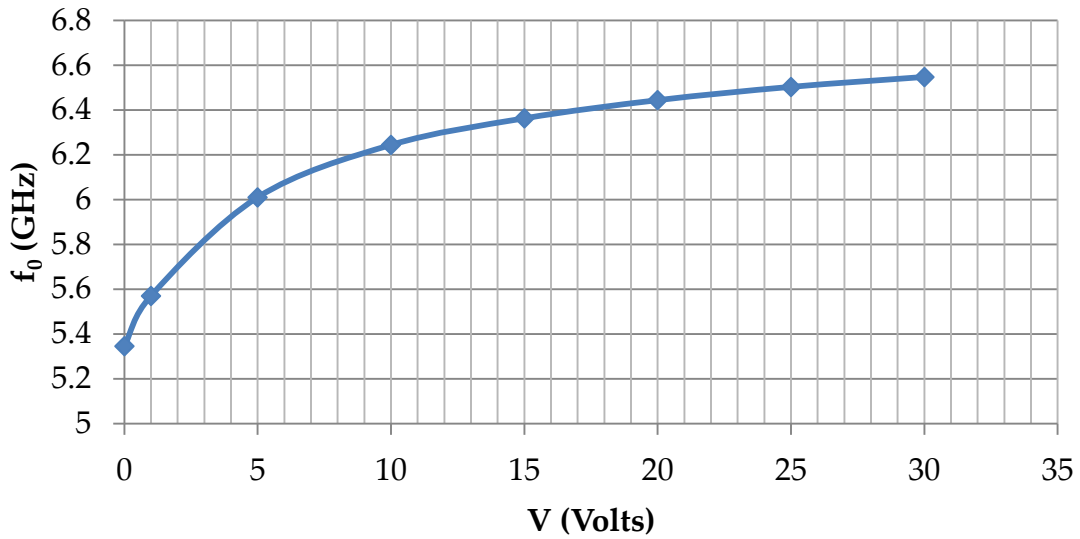
(a)
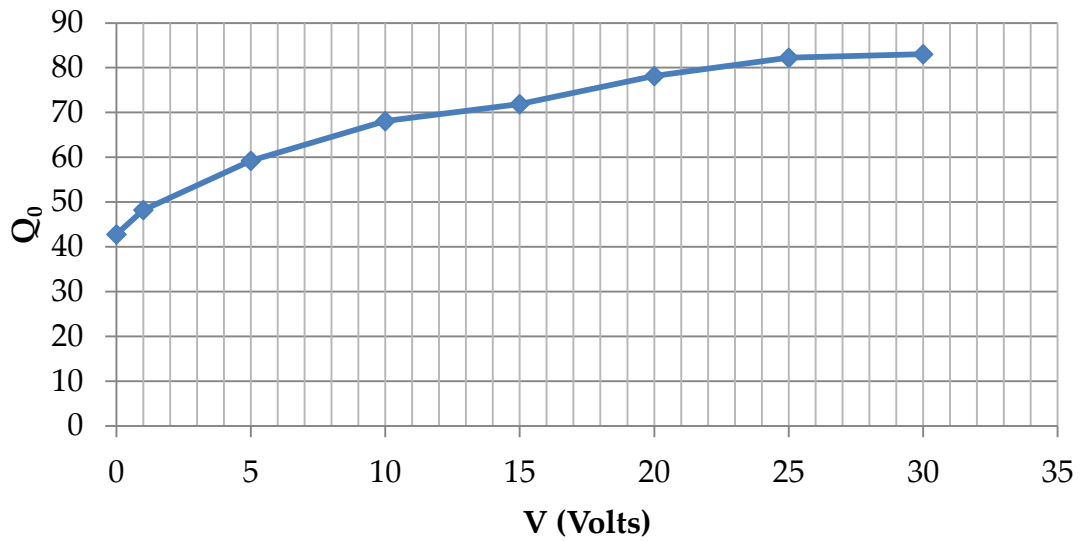
(b)

Figure 3.37 Commercial varactor tuning performance:

(a) center frequency versus voltage; (b) Q-factor versus voltage

Connecting two varactors in parallel, as shown in Figure 3.38, will provide a compromise between tuning range and Q. The tuning bandwidth decreased from 1.2 GHz to 771MHz for an average improvement in Q of 37%.
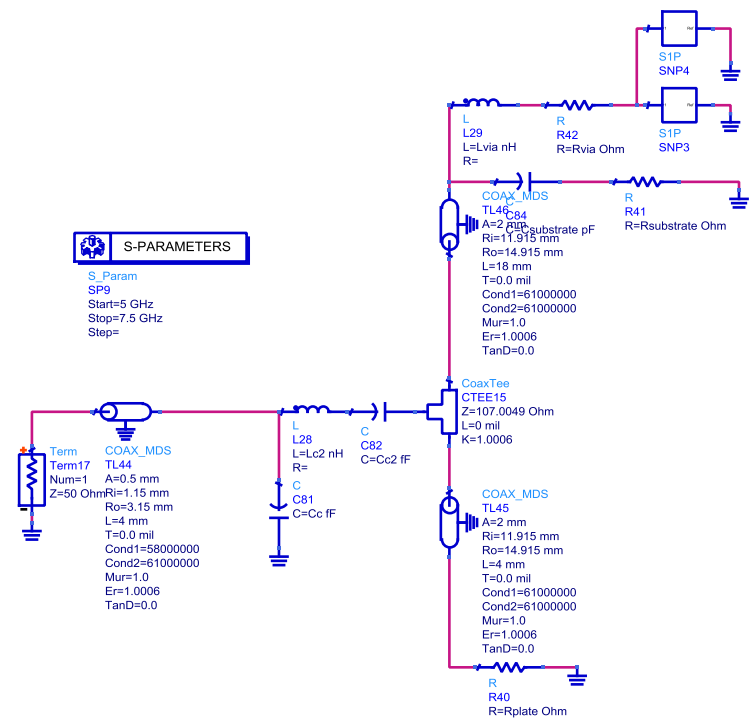
Figure 3.38 Two commercial varactors connected in parallel to a circuit model

A comparison between the performances of a single commercial varactor and two commercial varactors in parallel is shown in Figure 3.39.
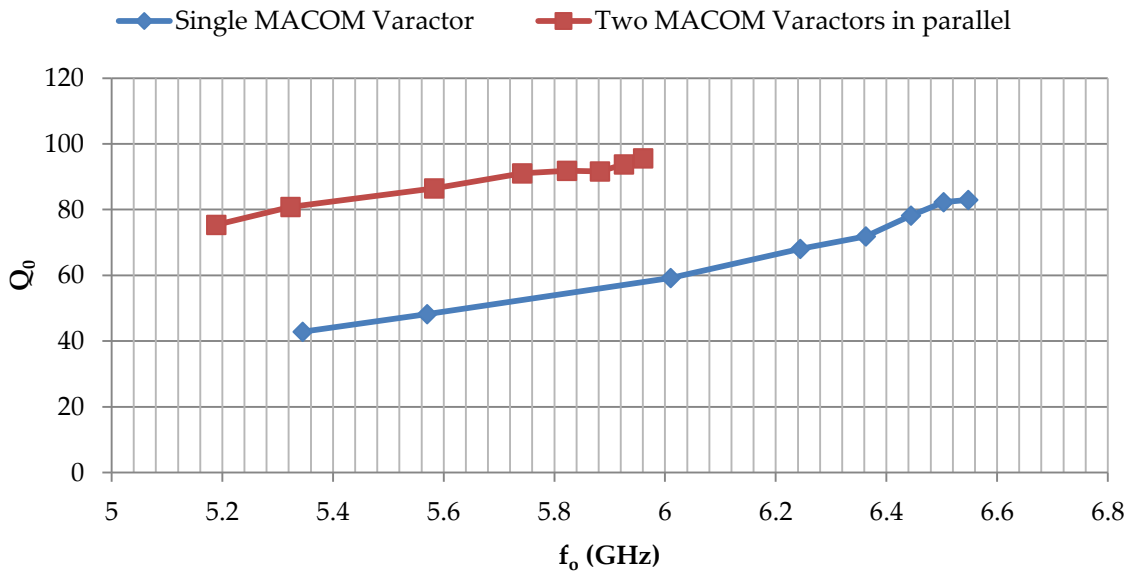
Figure 3.39 Q versus center frequency for coaxial resonator with a single varactor/two varactors in parallel connected to its top end

3.4 Summary

Two techniques for building an equivalent circuit model for 3D resonators were presented in this chapter. Both techniques were successfully tested and validated for different case studies. The performance of the node-to-node technique exceeded that of the lumped-element circuit model in many respects, such as allowing for the connecting of additional components that cannot be connected in an EM simulator and allowing other modes to be presented and considered. In addition, tunability was presented in such a way that it is in line with a sense of physicality. For example, adding a gap is equivalent to adding a capacitance.

Chapter 4

Novel Mechanically Tuned Filter Structure

The literature review in Chapter 2 presented an overview of some techniques used for tuning combline filters. This chapter presents the design and implementation of a high-Q bandpass filter using a novel tuning technique that maintains a constant Q value over a relatively wide tuning range [31].

The traditional technique for tuning combline filters is achieved by changing the gap between the post and the tuning disk. This technique is known to yield a Q value that degrades considerably at the lower edge of the tuning range. The proposed angular tuning technique shows a 25% improvement in the Q value at the lower edge of the tuning range, in comparison to what is typically achieved using the traditional tuning technique. Using the proposed angular tuning technique, a 1% bandwidth 2-pole filter is designed, fabricated, and tested with a 430MHz tuning range at a center frequency of 3.6 GHz. The insertion loss varies between 0.25 and 0.33dB. The filter is integrated with miniature piezoelectric motors, demonstrating an almost constant insertion loss over the tuning range.

4.1 Tunable Resonator

4.1.1 Structure

The combline resonator has a cavity of size 40cm × 40cm × 30cm, enclosing a cylindrical post with a diameter of 10 mm and a height of 15 mm. The tuning element is a rectangular sheet 12cm × 18cm attached to a vertical shaft. As shown in Figure 4.1, the center of the shaft is shifted from the post center position.
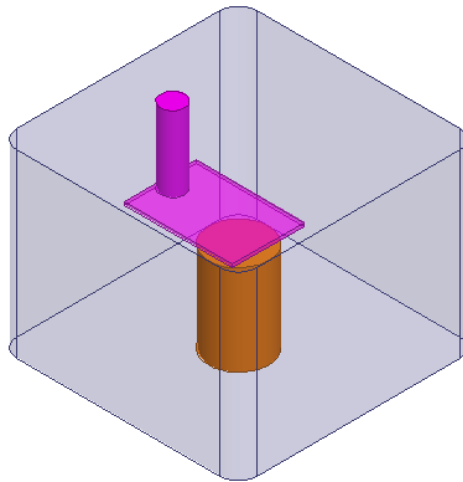
Figure 4.1 Single resonator

4.1.2 Angular tuning technique

The rectangular tuning element rotates radially around the vertical shaft's center. When the angle of rotation changes, the overlap area between the tuning element and the post will vary, which in turn tunes the center frequency without having much impact on the Q. Figure 4.2 shows the tuning element at different tuning positions.

(a)

(b)

(c)

(d)
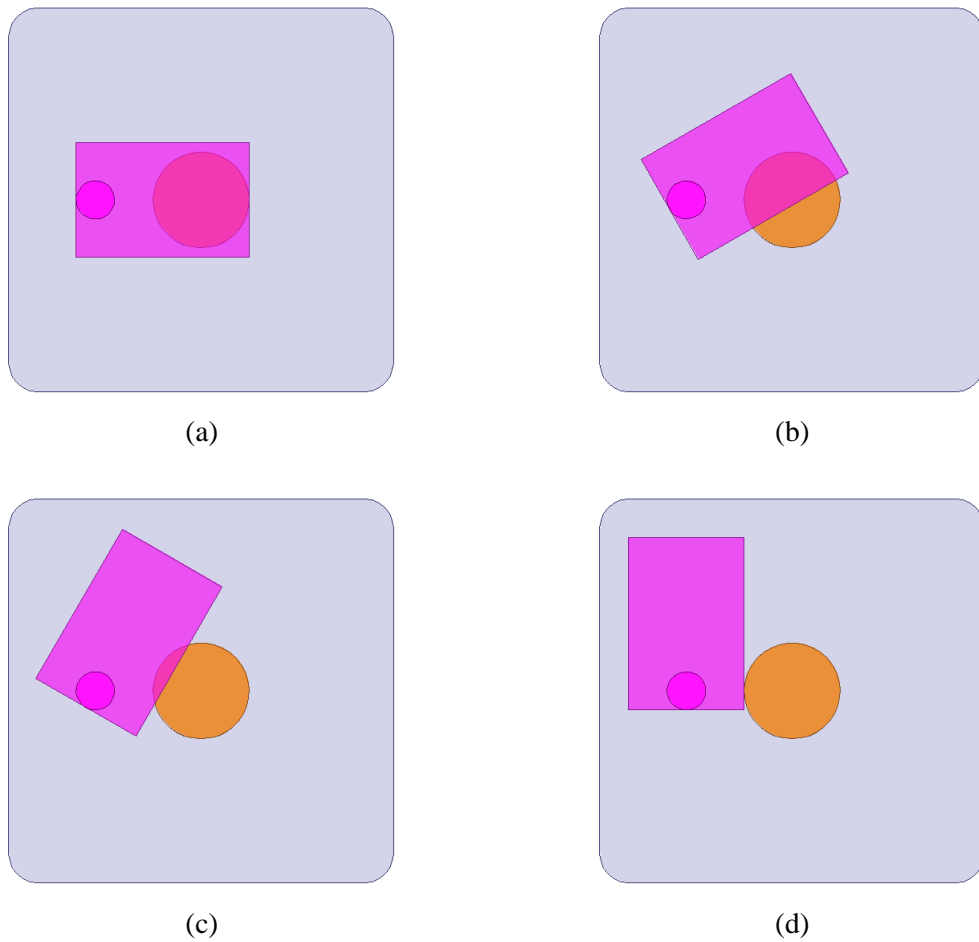
Figure 4.2 Angular tuning technique: (a) position at angle=0°; (b) position at angle=30°; (c) position at angle=60°; and (d) position at angle=90°

4.1.3 Comparison between angular tuning technique and traditional technique

To confirm that the proposed method far outperforms the traditional tuning technique in maintaining a constant Q over the tuning range, a comparison between two cavities tuned by the traditional method and the proposed method is carried out. Figure 4.3 shows the variation of frequency and Q for a combline cavity tuned using the proposed approach, whereas Figure 4.4 shows the combline resonator tuned using the traditional approach.
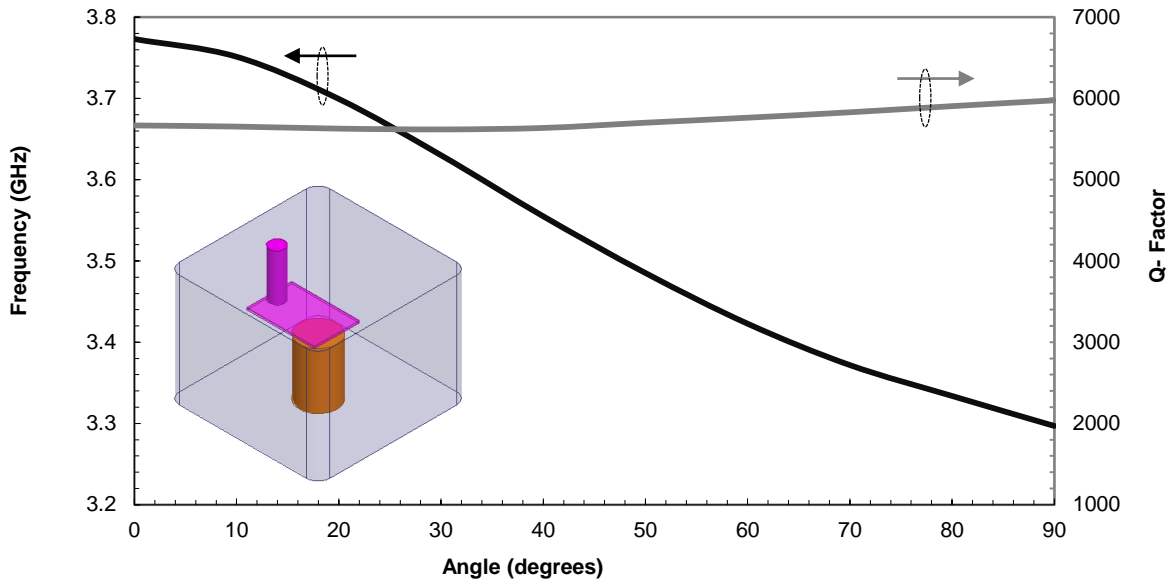
Figure 4.3 Simulation results for center frequency tuning and Q value of the proposed angular tuning technique
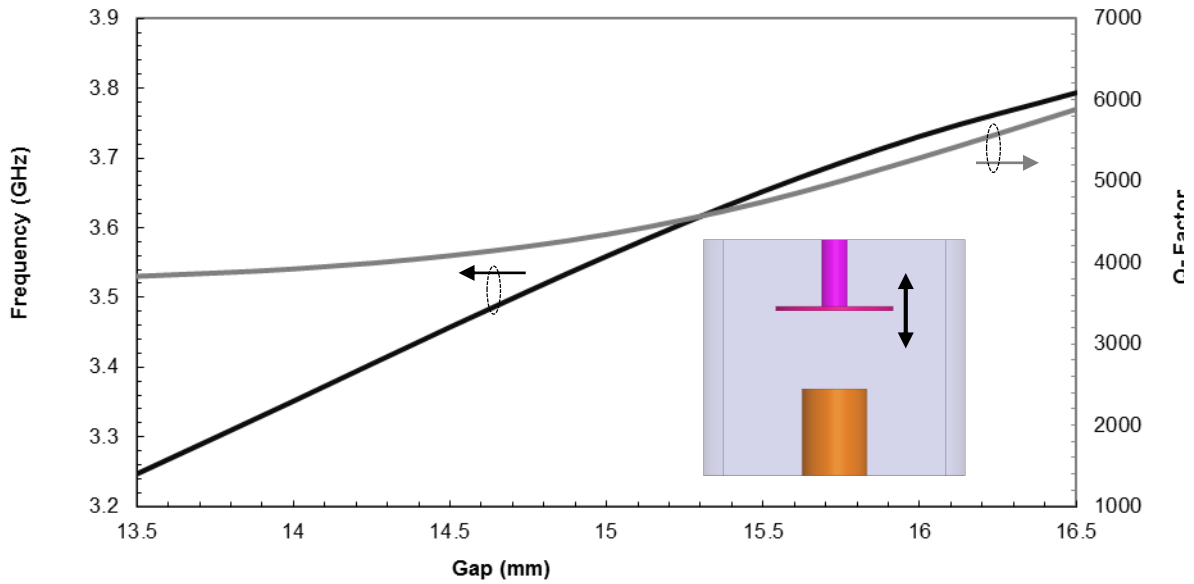
Figure 4.4 Simulation results for center frequency tuning and Q value traditional method of changing the disk penetration vertically

In viewing Figure 4.3 and Figure 4.4, it is evident that the angular tuning technique yields a significant improvement in the Q over the tuning range. For the angular tuning technique, the Q degradation is less than 6%, whereas the traditional approach of vertical tuning disk gives a degradation of 31% over the same tuning range. It should be noted that, in the above comparison, we maintained the same initial frequency and the same initial Q value. Table 4.8 shows the exact values obtained by the two techniques.

Table 4.8 A comparison between the proposed tuning approach and the traditional tuning approach for combline resonators

Tuning	Upper edge of the tuning range		Lower edge of the tuning range	
Technique	*Frequency*	*Q*	*Frequency*	*Q*
Traditional	3.77GHz	5640	3.29GHz	3881
Proposed	3.77GHz	5668	3.29GHz	5976

4.2 Tunable Filter Design

To verify the validity of the proposed concept, a 2-pole filter is designed, fabricated and tested. The filter is designed at 3.6 GHz with 430 MHz tuning range (11.9% tuning range).
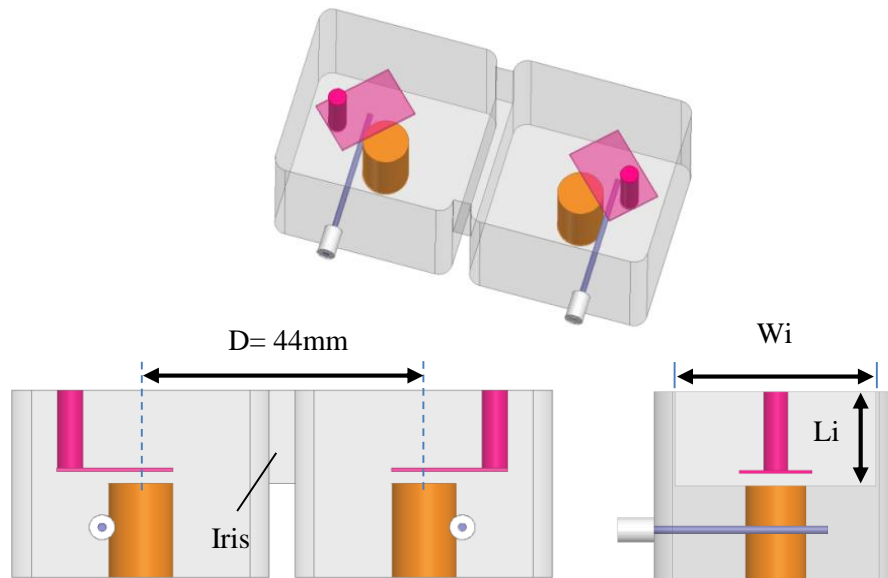
Figure 4.5 Simulation model of the 2-pole filter and iris dimensions

The filter dimensions were optimized to achieve an almost constant bandwidth over the tuning range. The iris dimensions are found to be 33mm and 13mm for W_i and L_i, respectively. Figure 4.5 shows the simulation model of the 2-pole filter.
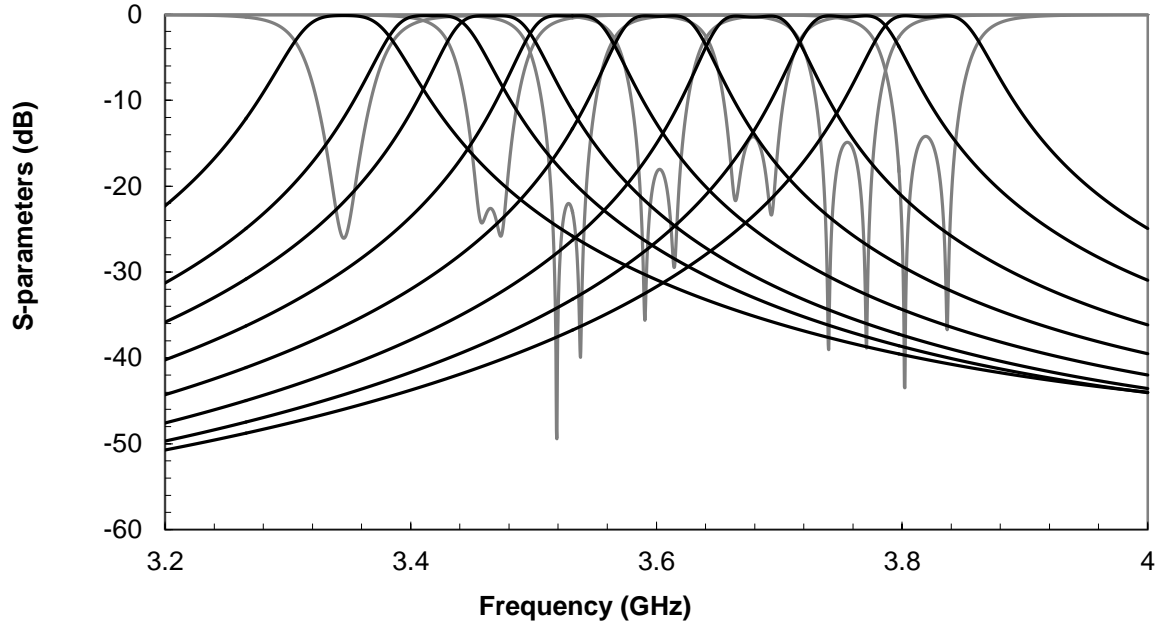
Figure 4.6 Simulated S-parameters of the designed filter

Figure 4.6 shows the HFSS simulation of the designed filter. The simulations show an almost constant IL value, ranging from 0.13dB to 0.32dB, with a return loss that is still acceptable over the 430MHz tuning bandwidth.

4.3 Fabrication and Measurement

The filter is fabricated out of copper. Coupling the tuning element to the motor is done using small aluminum parts, which slightly reduces the simulated Q-factor performance. Figure 4.7 shows the fabricated filter. Compact ultrasonic piezoelectric motors (PCB motor) are used on top of the filter [32].

The use of the angular tuning technique together with the PCB motors shrinks the overhead size of the filter [32]. This also makes the tuning straightforward and precise by adjusting the control of both motors. The mechanical movement is much more reliable in comparison to the traditional tuning approach of using special motors to drive the screws vertically.
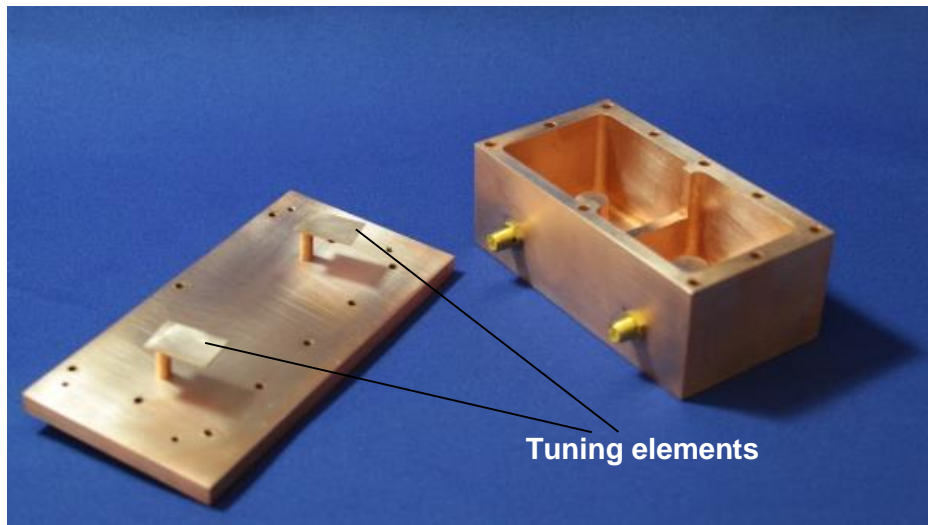
Tuning elements

(a)
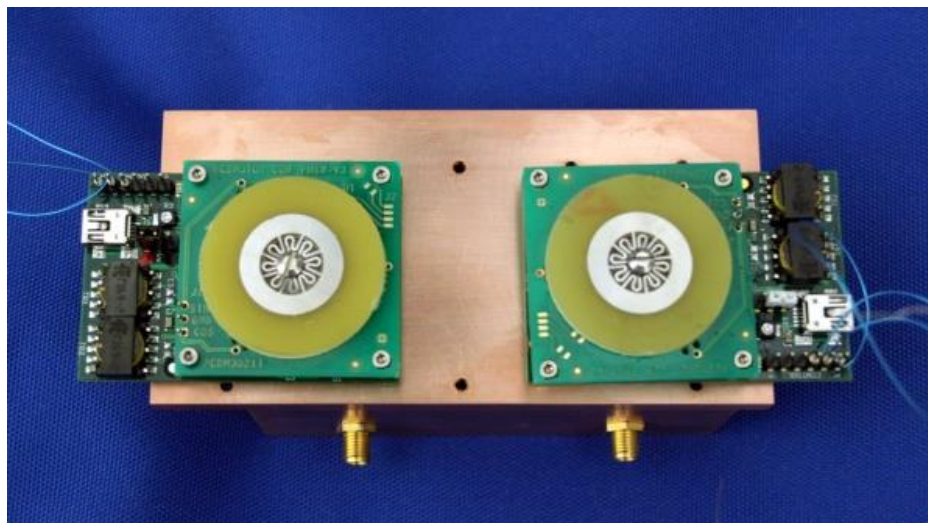
(b)

Figure 4.7 Fabricated filter: (a) angular tuning elements and filter body; (b) full setup showing the motors on top of the filter

The experimental results for the tunable filter with angular tuning, as shown in Figure 4.8, reveal an insertion loss variation of less than 0.11dB over the tuning range.
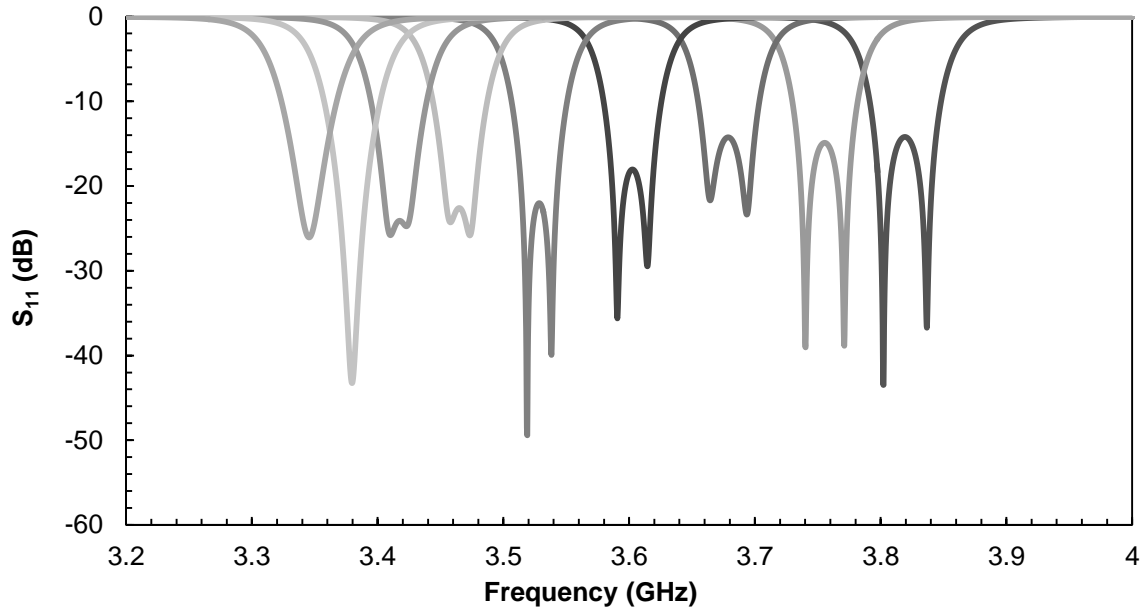
(a)
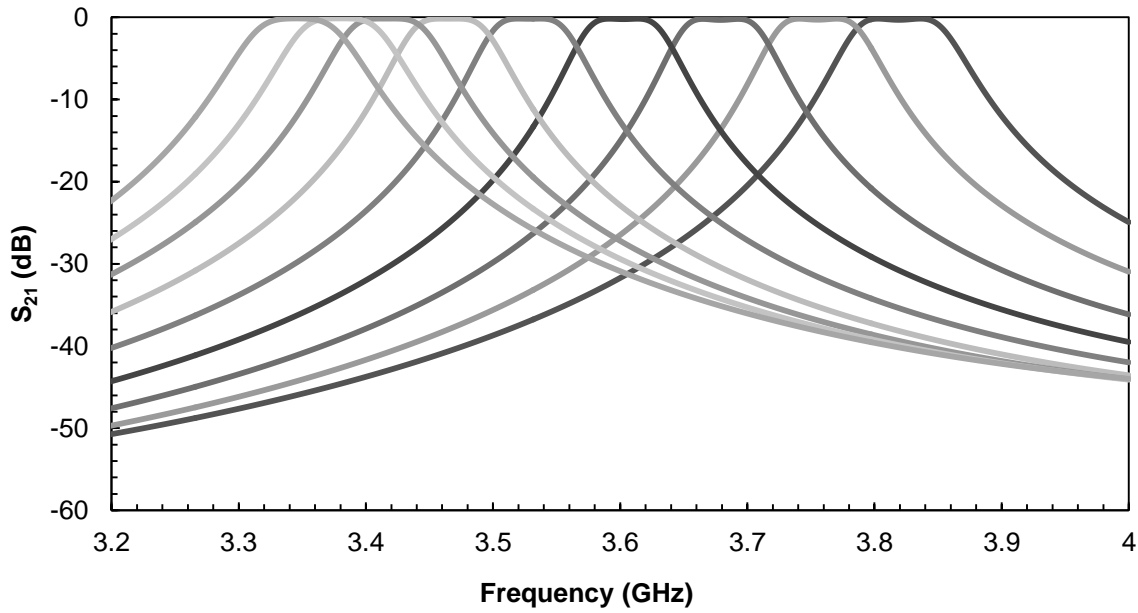
(b)

Figure 4.8 Measured S-parameters of the 2-pole tunable filter (a) S_{11} (b) S_{21}
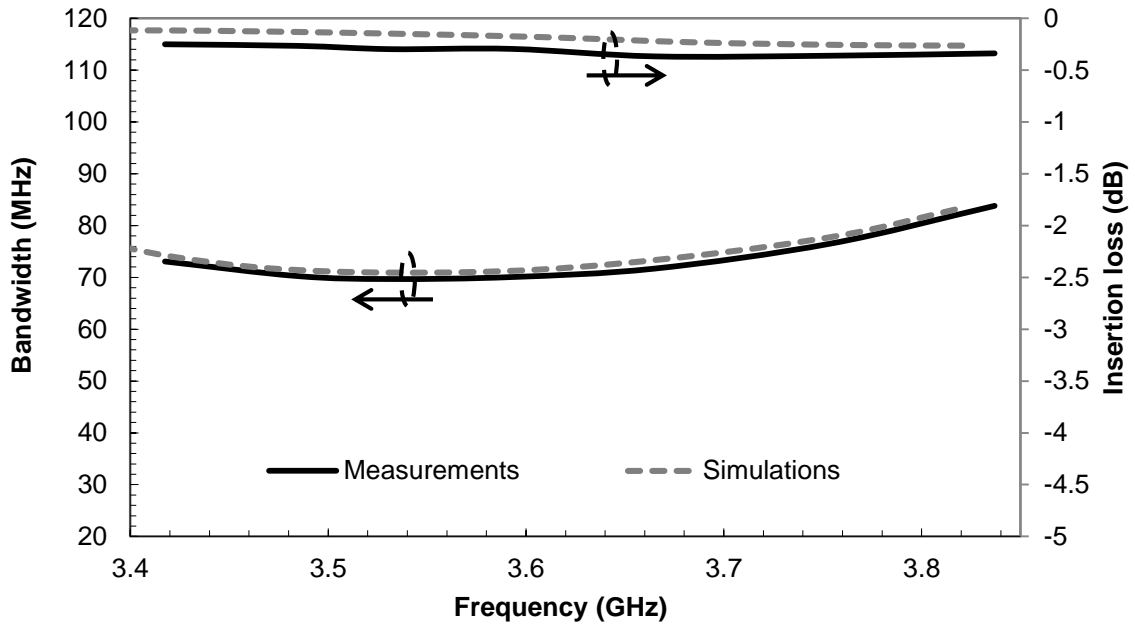
Figure 4.9 Insertion loss and 3-dB BW for simulated and measured data

Figure 4.9 shows the measured and simulated results for the insertion loss and 3-dB bandwidth. Experimental results are in line with the simulations. Over a tuning range of more than 400MHz, the insertion loss ranges between 0.25 to 0.36dB. The 3-dB bandwidth ranges from 70MHz to 83MHz over the tuning range.

4.4 Summary

A novel angular tuning technique was presented in this chapter. The technique was successfully employed to tune the filter with a constant high-Q within the 430MHz tuning range, centered at 3.6GHz (11.9% tuning range). An insertion loss degradation of less than 0.11dB and a 13MHz variation in 3-dB BW over a 430MHz tuning range were demonstrated using the novel technique. The use of compact motors had a positive effect on miniaturizing the overhead on top of the filter.

Chapter 5

Conclusions

To conclude this thesis, the contributions of this research are summarized and a few suggestions are provided for future study, based on the results achieved here.

5.1 Contributions

The primary contributions of this thesis are in two main areas:

- RF resonator equivalent circuit model:

  The thesis introduced two techniques to extract an equivalent circuit model for RF resonators. Both techniques were successfully tested and validated for different case studies. A lumped element technique was used to relate the EM model to an adjusted parallel RLC model that models the coupling. The node-to-node technique was based on using a transmission line equivalent to model combline resonators. It accounts for tunability, and directly and clearly represents the actual physical model. Several examples were given on how to apply the technique to gain greater insight into the factors that drive resonator performance and how to improve it.

- Angular tuning technique

  A novel angular tuning technique was used to mechanically tune the filter's center frequency. The technique was successfully employed to tune the filter with a constant high-Q within the 430MHz tuning range centered at 3.6GHz (11.9% tuning range). An insertion loss degradation of less than 0.11dB and a 13MHz variation in 3-dB BW over a 430MHz tuning range were demonstrated using the presented tuning technique.

5.2 Future Work

The node-to-node technique provides a tool that can be utilized to optimize the performance of electronic tuning using varactor diodes. The main problem is the varactor's internal resistance, which can be improved electronically by using a negative resistance circuit to cancel the varactor's internal resistance. All sorts of electronic simulation can be done now by virtue of the node-to-node technique.

Also, from the conclusions drawn from the first application of the node-to-node technique (section 3.3.3.1), we can try to engineer the way the substrate is connected to the coaxial resonator to reach minimal resistance and hence minimum degradation in the Q-factor. For example, the elimination of vias is expected to improve the Q value significantly.

Furthermore, the reason why the angular tuning technique outperforms the traditional tuning technique needs to be investigated by means of a thorough analysis. Developing such analysis should offer an insight providing a complete picture of the reasons behind Q degradation of such type of resonators.

Appendix A
List of Acronyms

RF	Radio Frequency
BST	Barium Strontium Titanate
MEMS	Microelectromechanical Systems
EM	Electromagnetic
HFSS	High Frequency Structural Simulator
ADS	Advanced Design System
BW	Bandwidth
Q	Quality factor
SMA	SubMiniature version A
CIRFE	Centre for Integrated RF Engineering

Appendix B
Motor Operation

In this section, we will go through the operation of the "Start Kit" from the PCBMotor company [32].The PCBMotor Start Kit is an ultrasonic piezoelectric motor consisting of the rotors mounted on either side of the stator board. Figure B.1 shows the motor from different views.

B.1 Powering the Motor

The motor gets its supply voltage V_{cc}, from the +5V pin in the USB mini connector. This will result in a rotational speed of around 0.8 revolutions per second and a motor supply current of typically 200mA. Increasing the motor voltage increases the speed of the travelling current. The current should be kept below 480mA for a 30mm start to avoid motor damage.

B.2 Controlling Start/Stop & CW/CCW rotation

After powering up the motor, it is normally on standby mode. To start running the motor, pin #2 should be pulled low, as shown in Table B.1. The motor will rotate by default in a counter-clock-wise direction. To change the direction of rotation to clock-wise, pin #1 should be pulled low.

Table B.1 Control pins

Pin No.	High or n.c.	Pulled low
Pin 2 : STB	Standby	Run
Pin 1 : SEL	CCW	CW

B.3 Mechanical Connection

The spring in the center of the upper rotor presses both rotors towards the stator. Ideally, the mechanical design should ensure that the rotor only transfers rotational forces to the axle. However, a load of 75-150g, mounted directly onto the rotor should be fine if the motor axle is vertical.

If the motor axle is horizontal, the mechanical load could make the rotors tilt, whereby some of the piezo elements could lose contact with the rotors. This would reduce motor performance and increase acoustical noise level.

B.4 On-board Sensor

The Start Kit includes some of the basic elements of a positioning system, namely an encoder and a sensor. The encoder is an etched copper pattern on one of the rotors and the resolution is 200 steps

per revolution. The sensor is a reflective object sensor consisting of a light source sending constant light towards the encoder and a photo transistor detecting the reflected light. The TTL level output of the sensor is available at pin 6. This output can be used to do a closed-loop positioning for both motors. This will help in obtaining the same angle of rotation for both motors when starting at the same initial position.
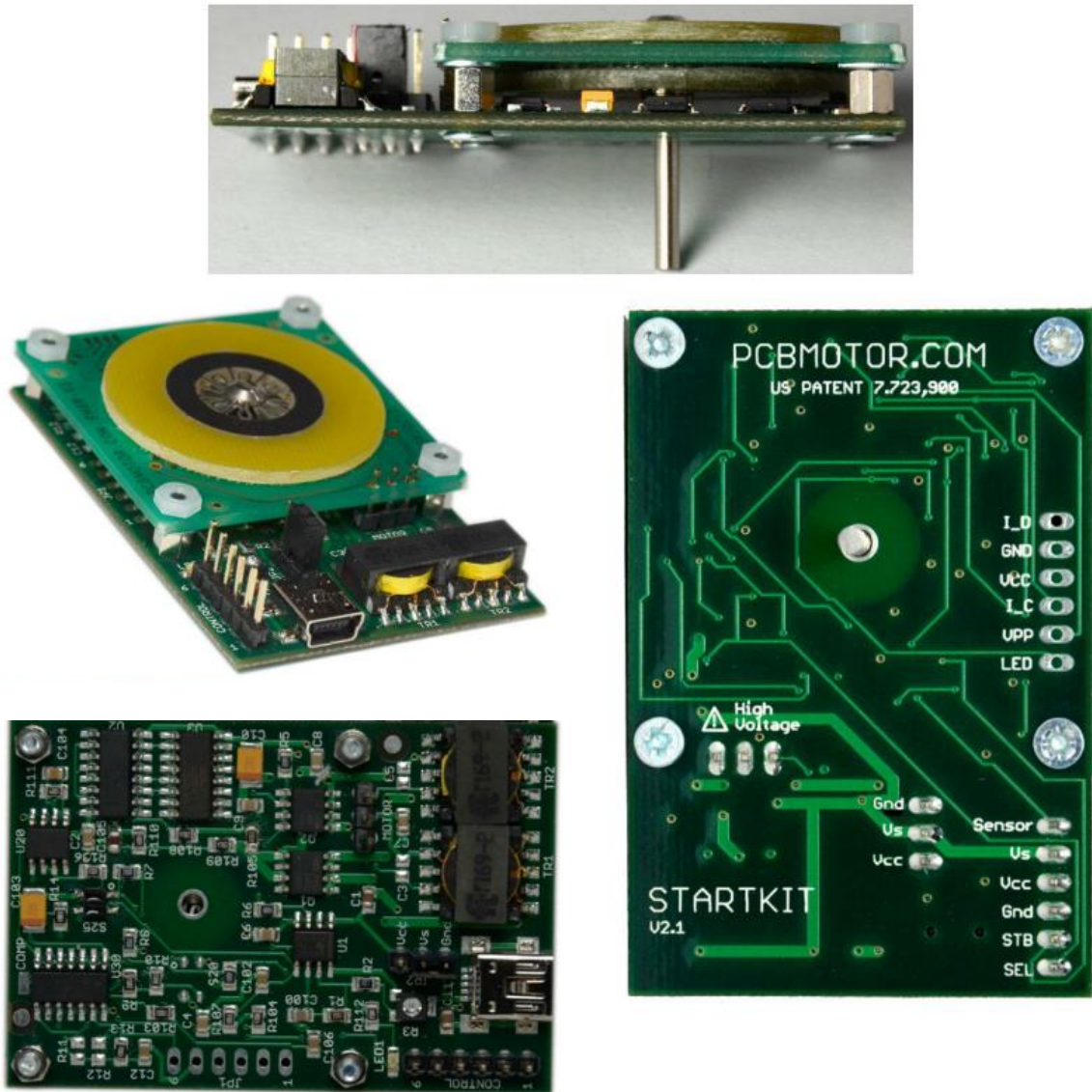
Figure B.1 PCB Motor from different views

B.5 Specifications

The motor mechanical and electrical specifications can be found in Table B.2.

Table B.2 Motor Mechanical and Electrical Specifications

Temperature range	-20 to +50 degrees Celsius
Supply voltage	+5V via USB A / USB mini B cable
Supply current	Typ. 200 mA when motor is ON
Max. motor current	480 mA
Maximum stall torque	Typ. 25 Nmm
Maximum speed of rotation	Typ. 1.3 rps

Bibliography

[1]   R. R. Mansour, "RF filters and diplexers for wireless system applications: state of the art and trends," in *Radio and Wireless Conference, 2003. RAWCON'03. Proceedings*, pp. 373–376, IEEE, 2003.

[2]   A. S. Hussaini, R. Abd-Alhameed, and J. Rodriguez, "Tunable RF filters: Survey and beyond," in *Electronics, Circuits and Systems (ICECS), 2011 18th IEEE International Conference on*, pp. 512–515, IEEE, 2011.

[3]   J. Uher and W. J. Hoefer, "Tunable microwave and millimeter-wave band-pass filters," *Microwave Theory and Techniques, IEEE Transactions on*, vol. 39, no. 4, pp. 643–653, 1991.

[4]   S. Fouladi, F. Huang, W. D. Yan, and R. R. Mansour, "High- Narrowband Tunable Combline Bandpass Filters Using MEMS Capacitor Banks and Piezomotors," *Microwave Theory and Techniques, IEEE Transactions on*, vol. 61, no. 1, pp. 393–402, 2013.

[5]   S.-W. Chen, K. A. Zaki, and R. G. West, "Tunable, temperature-compensated dielectric resonators and filters," *Microwave Theory and Techniques, IEEE Transactions on*, vol. 38, no. 8, pp. 1046–1052, 1990.

[6]   T. Shen, K. A. Zaki, and C. Wang, "Tunable dielectric resonators with dielectric tuning disks," *Microwave Theory and Techniques, IEEE Transactions on*, vol. 48, no. 12, pp. 2439–2445, 2000.

[7]   G. I. Panaitov, R. Ott, and N. Klein, "Dielectric resonator with discrete electromechanical frequency tuning," *Microwave Theory and Techniques, IEEE Transactions on*, vol. 53, no. 11, pp. 3371–3377, 2005.

[8]   T.-Y. Yun and K. Chang, "Piezoelectric-transducer-controlled tunable microwave circuits," *Microwave Theory and Techniques, IEEE Transactions on*, vol. 50, no. 5, pp. 1303–1310, 2002.

[9]   M. Al-Ahmad, R. Matz, and P. Russer, "Piezoelectric tuned LTCC bandpass filters," in *Microwave Symposium Digest, 2006. IEEE MTT-S International*, pp. 764–767, IEEE, 2006.

[10]   S. Hontsu, K. Iguchi, K. Agemura, H. Nishikawa, and M. Kusunoki, "Mechanical Tuning of Superconducting Lumped," vol. 15, no. 2, pp. 972–975, 2005.

[11]   W. Keane, "Narrow-band YIG filters aid wide-open receivers," *Microwaves*, vol. 17, pp. 50–54, 1978.

[12]   J. Krupka, A. Abramowicz, and K. Derzakowski, "Magnetically tunable filters for cellular communication terminals," *Microwave Theory and Techniques, IEEE Transactions on*, vol. 54, no. 6, pp. 2329–2335, 2006.

[13]   I. Hunter and J. D. Rhodes, "Electronically tunable microwave bandpass filters," *Microwave Theory and Techniques, IEEE Transactions on*, vol. 30, no. 9, pp. 1354–1360, 1982.

[14]   A. R. Brown and G. M. Rebeiz, "A varactor-tuned RF filter," *Microwave Theory and Techniques, IEEE Transactions on*, vol. 48, no. 7, pp. 1157–1160, 2000.

[15]   M. Sánchez-Renedo and J. I. Alonso, "Tunable planar combline filter with multiple source/load coupling," in *Microwave Symposium Digest, 2005 IEEE MTT-S International*, p. 4, IEEE, 2005.

[16]   F. Huang and R. Mansour, "A novel varactor tuned dielectric resonator filter," in *Microwave Symposium Digest (IMS), 2013 IEEE MTT-S International*, pp. 1–3, IEEE, 2013.

[17]   A. Tombak, J.-P. Maria, F. T. Ayguavives, Z. Jin, G. T. Stauf, A. I. Kingon, and A. Mortazawi, "Voltage-controlled RF filters employing thin-film barium-strontium-titanate tunable capacitors," *Microwave Theory and Techniques, IEEE Transactions on*, vol. 51, no. 2, pp. 462–467, 2003.

[18]   G. Sanderson, A. H. Cardona, T. Watson, D. Chase, M. Roy, J. Paricka, and R. York, "Tunable IF filter using thin-film BST varactors," in *Microwave Symposium, 2007. IEEE/MTT-S International*, pp. 679–682, IEEE, 2007.

[19]   Y.-H. Chun, J.-S. Hong, P. Bao, T. J. Jackson, and M. J. Lancaster, "BST-varactor tunable dual-mode filter using variable transmission line," *Microwave and Wireless Components Letters, IEEE*, vol. 18, no. 3, pp. 167–169, 2008.

[20]   M.-T. Nguyen, W. D. Yan, and E. P. Horne, "Broadband tunable filters using high q passive tunable ICs," in *Microwave Symposium Digest, 2008 IEEE MTT-S International*, pp. 951–954, IEEE, 2008.

[21]   J. Nath, D. Ghosh, J.-P. Maria, A. I. Kingon, W. Fathelbab, P. D. Franzon, and M. B. Steer, "An electronically tunable microstrip bandpass filter using thin-film Barium-Strontium-Titanate (BST) varactors," *Microwave Theory and Techniques, IEEE Transactions on*, vol. 53, no. 9, pp. 2707–2712, 2005.

[22]   K. Entesari, K. Obeidat, A. R. Brown, and G. M. Rebeiz, "A 25–75-MHz RF MEMS tunable filter," *Microwave Theory and Techniques, IEEE Transactions on*, vol. 55, no. 11, pp. 2399–2405, 2007.

[23]   I. Reines, A. Brown, M. El-Tanani, A. Grichener, and G. Rebeiz, "1.6-2.4 GHz RF MEMS tunable 3-pole suspended combline filter," in *Microwave Symposium Digest, 2008 IEEE MTT-S International*, pp. 133–136, IEEE, 2008.

[24]   S.-J. Park and G. M. Rebeiz, "Low-loss two-pole tunable filters with three different predefined bandwidth characteristics," *Microwave Theory and Techniques, IEEE Transactions on*, vol. 56, no. 5, pp. 1137–1148, 2008.

[25]   M. A. El-Tanani and G. M. Rebeiz, "High-performance 1.5–2.5-GHz RF-MEMS tunable filters for wireless applications," *Microwave Theory and Techniques, IEEE Transactions on*, vol. 58, no. 6, pp. 1629–1637, 2010.

[26]   R. Owens, "Equivalent-circuit parameters of a cavity resonator," *Electronics Letters*, vol. 3, no. 7, pp. 327–328, 1967.

[27]   M. Toman and T. K. Ishii, "Equivalent-circuit parameters of a cylindrical-cavity resonator," *Electronics Letters*, vol. 3, no. 1, pp. 36–38, 1967.

[28]   W. Wheless and D. Kajfez, "Microwave resonator circuit model from measured data fitting," in *Microwave Symposium Digest, 1986 IEEE MTT-S International*, pp. 681–684, IEEE, 1986.

[29]   S. Simion, "Dielectric resonator equivalent circuit," *Proceedings of MELECON '94. Mediterranean Electrotechnical Conference*, pp. 488–491, 1994.

[30]   Internal communication with Oliver Wong.

[31]   M. A. Iskander, M. Nasresfahani, and R. R. Mansour, "A constant-Q tunable combline bandpass filter using angular tuning technique," in *Microwave Conference (EuMC), 2014 European*, IEEE, 2014 (Accepted).

[32]   http://www.pcbmotor.com.

[33]   R. J. Cameron, C. M. Kudsia, and R. R. Mansour, *Microwave filters for communication systems*. Wiley-Interscience, 2007.